Measurement Notes

Note 19

Estimation of Errors in Calculating Transfer Functions from Pulse Data

by
Chris Ashley
and
William R. Graham

5 September 1973

Air Force Weapons Laboratory
and
R & D Associates

Abstract

Analysis of responses of linear systems, or of linear subsystems within larger systems, to transient stimuli commonly involves the concept of transfer functions. Estimation, verification, and use of these transfer functions often entails recording of transient stimuli and transient system response. These data are then digitized and processed numerically to produce the transfer function. The recording and digitization processes are usually the most important sources of error in the transfer function measurement. Conclusions drawn about the systems being analyzed are correspondingly in error. The purpose of this paper is to discuss some ways of estimating the magnitudes of the important errors in the data reduction process and to show how errors in the transfer function are related to errors in that process.

Contents

Estimation of Errors in Calculating Transfer Functions from Pulse Data.

Part I. Introduction.

1. The purpose of this paper is to present a procedure which will, hopefully, aid in understanding the response of linear systems, or linear parts of more complicated systems, to transient stimuli.

2. A linear system is a system which has the property that, if a stimulus $f_1(t)$ (t for time) produces a response $g_1(t)$ and stimulus $f_2(t)$ produces response $g_2(t)$, then stimulus $af_1(t)+bf_2(t)$ will produce response $ag_1(t)+bg_2(t)$ for any two scalars a and b.[1] The linear system (or subsystem) may be represented schematically as a single-input-single-output box, thus:

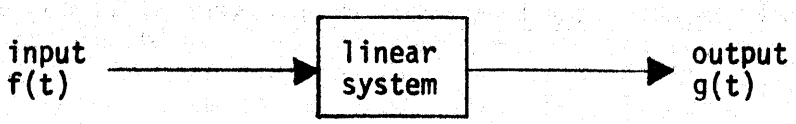

Figure 1.

For example, the input and output may be electrical signals.

3. Why are we interested in the responses of linear systems to transient stimuli? Briefly, we want to know whether an undesired transient stimulus might produce a response of such great magnitude as to damage or disrupt normal operation of the next system (or subsystem) in the chain. For example, if we could predict the response of Subsystem A in Figure 2 to a particular stimulus, and if we knew the threshhold of damage or disruption of Subsystem B, then we could predict whether normal operation of Subsystem B would be disturbed as a result of the incidence of that particular stimulus function on Subsystem A.

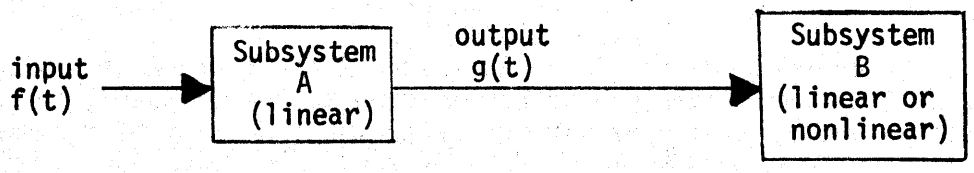

Figure 2.

4. One might ask why we are restricting the enquiry to subsystems A which are linear; why not investigate also those which are nonlinear? First, the linear subsystem can be used to provide a simple but illustrative example of a more general method for estimating several types of experimental error. Second, a great many of the real problems of interest happen to satisfy the restriction, and so can be adequately represented by Figure 2.

5. For example, consider the problem of an electrical system which includes a digital computer. An electromagnetic field pulse originating outside the system might be able to produce spurious electrical currents on the wires which carry normal input data to the computer. To prevent the computer from mistakenly interpreting these spurious currents as legitimate input data and attempting to operate based on them, it is common practice (where such external fields are possible and error free operation is important) to surround the computer and the conductors leading to it by conductive shielding. Unfortunately such shielding arrangements can in day to day use develop weaknesses which go undetected in the absence of disrupting external fields, for example at the conductive seam, weld, or connector joining the shielding of the computer with the shielding of the conductors which bring input to it. In this case Figure 2 becomes:

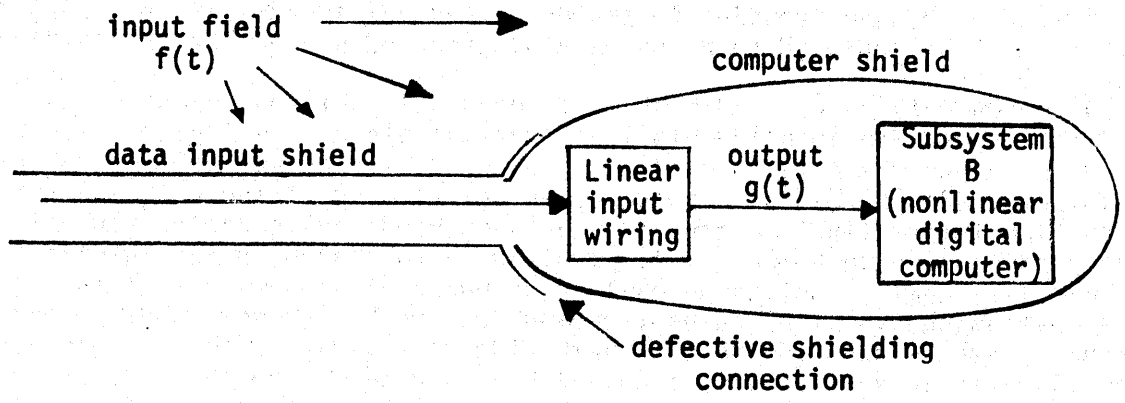

Figure 3.

What in Figure 3 corresponds to linear Subsystem A of Figure 2 is all of the shielding, the simple data conductors leading to the computer, and any more complicated but still linear wiring at the input section of the computer.

6. (The transfer function.) It can be proved[2] mathematically directly from the definition of linearity given in paragraph 2 that there exists a function

$h(t)$, which depends upon the features of the linear system in Figure 1 but which is independent of the stimulus $f(t)$, such that

$$g(t) = \int_{-\infty}^{\infty} f(\tau)\, h(t-\tau)\, d\tau \qquad (1)$$

provided the system is time invariant. Therefore there exists a mathematical model (viz., $h(t)$) for what the system does to any physically realizable input $f(t)$ to produce $g(t)$. If we can discover $h(t)$ for the particular system of interest, therefore, we will understand completely the response $g(t)$ of that system to any real input stimulus $f(t)$.

7. By another theorem[3] in mathematics, equation (1) can be rewritten

$$G(\omega) = F(\omega) * H(\omega) \qquad (2)\ ,$$

where $F(\omega)$ is the Fourier transform of $f(t)$, given by

$$F(\omega) \triangleq \int_{-\infty}^{\infty} f(t)\, e^{-i\omega t}\, dt \qquad (3)\ ,$$

and $G(\omega)$ and $H(\omega)$ similarly are the Fourier transforms of $g(t)$ and $h(t)$, respectively. Solving equation (2) for $H(\omega)$ yields immediately

$$H(\omega) = \frac{G(\omega)}{F(\omega)} \qquad (4)\ .$$

Knowing $H(\omega)$ from equation (4) we can inverse Fourier transform[4] to get

$$h(t) = \frac{1}{2\pi} \int_{-\infty}^{\infty} H(\omega)\, e^{i\omega t}\, d\omega \qquad (5)\ .$$

8. Our objective is to gain enough understanding of a particular linear system, or linear subsystem, so that we may predict what response $g(t)$ will

result from a specified transient stimulus $f(t)$ (cf. Figure 1). Since we know that for linear systems the transfer function $h(t)$ (and $H(\omega)$) is independent of $f(t)$ (cf. paragraph 6, above), one obvious idea for attaining our objective is to use the following procedure.

I. Put some arbitrary test stimulus $\tilde{f}(t)$ into the linear system (or linear subsystem).

II. Record both $\tilde{f}(t)$ and the resulting $\tilde{g}(t)$ (cf. Figure 1).

III. Perform the operation represented by equation (3), for example numerically in a digital computer, to get $\tilde{F}(\omega)$ and $\tilde{G}(\omega)$.

IV. Calculate the linear system transfer function $H(\omega)$ from equation (4).

V. Then, for any other transient stimulus $f(t)$, perform the operation represented by equation (3) to get $F(\omega)$.

VI. Calculate the linear system response $G(\omega)$ from equation (2).

VII. Perform the operation represented by equation (5), for example numerically in a digital computer, to get the linear system (or subsystem) response $g(t)$ to stimulus $f(t)$.

In fact, this procedure is commonly used. Some variations on it are also used. One variation, CW (continuous wave) testing, replaces steps I, II, and III, above, with the following two steps.

I′. Into the linear system (or linear subsystem) put a sinusoidal stimulus $f(t) \equiv A(\omega)\sin(\omega t)$ of constant frequency and constant peak amplitude. For a linear system (or linear subsystem) the response will be of the form $g(t) = B(\omega)\sin(\omega t - \phi(\omega))$.[5]

II′. For each ω record both the magnitude $A(\omega)$ of the stimulus and the magnitude $B(\omega)$ and phase shift $\phi(\omega)$ of the response.

These two steps supply $F(\omega)$ (= $(A(\omega),0)$, in polar coordinates) and $G(\omega)$ (= $(B(\omega),\phi(\omega))$) directly for use by step IV. Another variation, time domain unfolding, replaces steps V, VI, and VII, above, with the following two steps.

V′. Calculate the linear system transfer function $h(t)$ from equation (5).

VI′. Then, for any other transient stimulus $f(t)$, calculate the response $g(t)$ of the linear system (or linear subsystem) from equation (1).

Yet a third variation is simply to apply both the preceding two variations simultaneously, i.e., perform steps I′, II′, IV, V′, and VI′.[6]

9. It turns out that these procedures are more easily stated than executed.

Part II. The problem.

10. Unfortunately, the procedures outlined in paragraph 8, above, don't yield quite the right transfer function $H(\omega)$ (or $h(t)$) nor, therefore, the correct new response $g(t)$. This is because there are sources of error implicit in the procedures. For example, there is experimental error in the process of instrumenting $\tilde{f}(t)$ and $\tilde{g}(t)$ (or $\tilde{F}(\omega)$ and $\tilde{G}(\omega)$). Then, since equations (3) and (5) are usually evaluated numerically, the functions are usually sampled and digitized. Sampling and digitizing can be done directly from the signal, recording then only the digital samples. However, for EMP (electromagnetic pulse) information in the past more often sampling and digitizing have been done after recording the analogue signal, from a polaroid photograph of an oscilloscope trace. In the latter case a second source of error is the recording process, and digitizing is a third. The sample points are then reconnected, explicitly or implicitly, by some analytically transformable function. This analytic interpolation generally does not have quite the same values between the digitized sample points as did the original experimental function, so a fourth error is incurred in interpolation. The numerical evaluation of the analytic transform of the interpolation is a fifth source of error, because of round off for example.

11. This list of error sources for the procedures discussed in paragraph 8 is by no means complete. Appendix A gives a more complete, though still not exhaustive, list of sources of system test data distortion for a system appraisal apparatus much used to date. Such lists can be made impressively long. Even after considerable effort has been spent in minimizing the individual errors, the remaining cumulative error can be significant. For example, consider just the errors from sources numbered 12., 13., and 14. in Appendix A, i.e., the error induced in calculating transfer functions, as functions of frequency, from data photographs where the photographs are assumed to be error free. An experiment which one might perform is to reduce the data from such photographs to a transfer function, then repeat the reduction using the same data photographs to see if he gets the same transfer function the second time. This experiment has in fact been performed[7], using operational and trusted data reduction equipment and procedures. The reduction was performed forty-five times, using repeatedly the same actual data photographs. Figure 4 shows the greatest and least magnitudes calculated for the transfer function at each frequency. Thus the spread between the two graphs in Figure 4 gives an indication of the amount of non-repeating error which sources 12., 13., and 14. in Appendix A can cause in the performance of just steps III and IV in the first procedure in paragraph 8, above. The figure shows these errors can distort the calculated transfer function amplitude into values ranging over a factor of 10 at low frequencies, a factor of 20 at nulls, and a factor of 200 at high frequencies. Where between these extremes is the "true" transfer function amplitude at each frequency? Where with respect to any one of the calculated amplitudes is the truth at each frequency? It would seem from this example that data reduction random error can be significant. Consequently it would seem the problem of estimating this error is worth solving. The purpose of this paper is to propose a way to solve this problem.

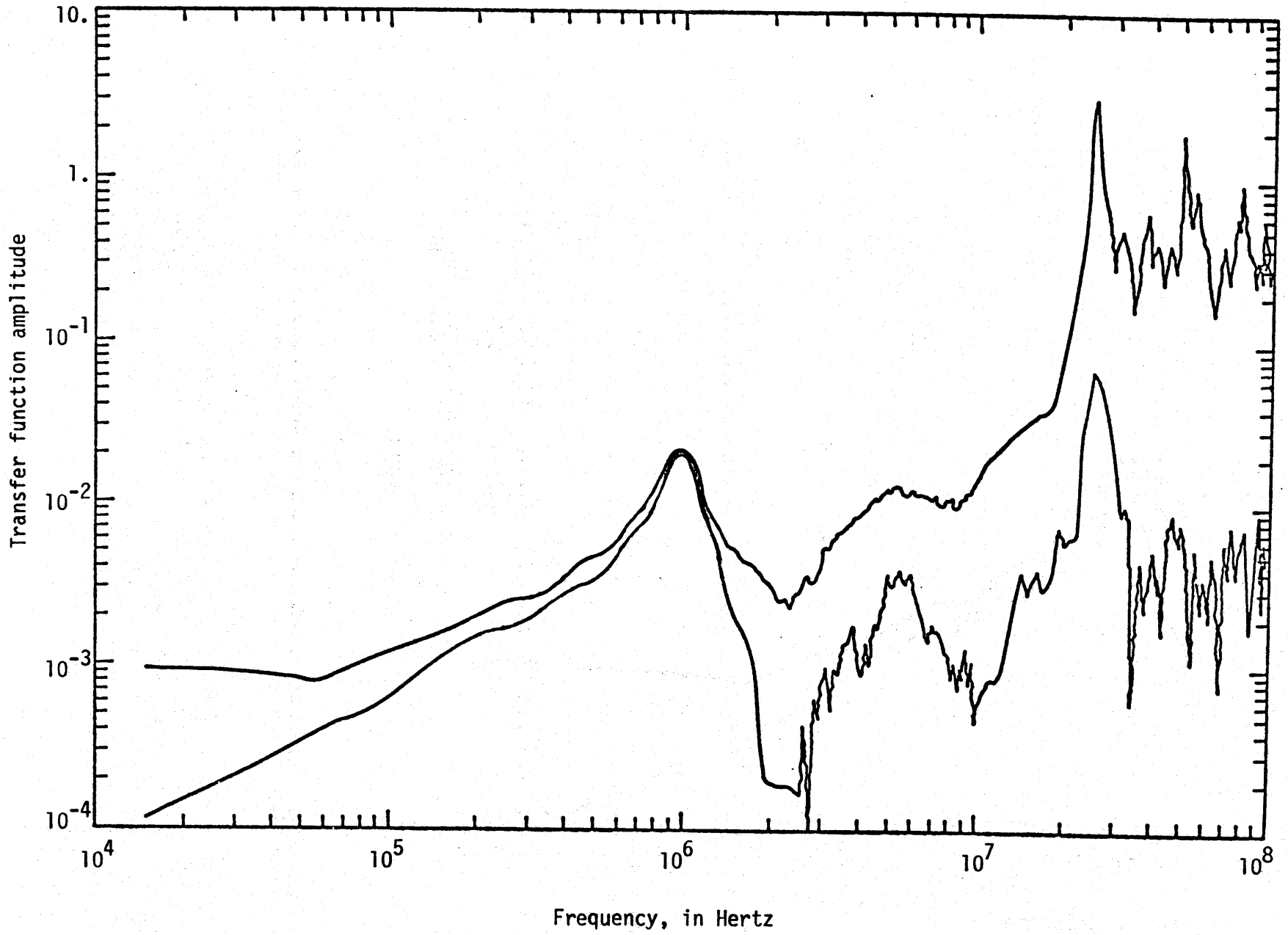
10.
1.
10^{-1}
10^{-2}
10^{-3}
10^{-4}
Transfer function amplitude
10^4
10^5
10^6
10^7
10^8
Frequency, in Hertz

Figure 4.

Part III. Approaches to the problem.

12. How is the cumulative error from the sources in Appendix A to be estimated? One way is the variables analysis approach, described in Appendix B. (Cf. also paragraph 19, following.) This approach has been used in the analysis of several systems in the past. It has the advantage that it provides an estimate of error applicable generally to gross classes of system data and performance predictions. On the other hand, the error estimates which come from variables analysis are usually not tailored to individual pieces of data, and so may be inapplicable and inaccurate, or at best too conservative, in specific cases. Therefore, although the variables analysis solution to error estimation is useful, techniques more precisely tailored to individual data are needed also. The purpose of this paper is to present one such technique for solving the error estimation problem.

13. Our idea for helping solve the problem of estimating the error in the output of the procedures outlined in paragraph 8, above, is to enable the computer which reduces the data also to simulate the random behavior of some of the processes and equipment used in the procedures. To illustrate this computer simulation technique in detail, we will assume a specific system analysis procedure and a specific sequence of data gathering and processing procedures. The system analysis procedure which we will use will be that stated in paragraph 8, above, minus the variations suggested there. The sequence of data gathering and processing procedures will be those cited in paragraph 10, above, using the second option of when to digitize (since most of the system EM pulse data presently on hand was taken that way). Therefore the sources of the errors which we will try to simulate are to a large extent contained in Appendix A. Specifically, we will try to simulate most of the random errors introduced in steps II through IV, inclusive, in paragraph 8, i.e., by sources 10. through 14., inclusive, plus source 15.D., in Appendix A. (We believe the idea of computer simulation of error could be extended to other error sources besides these.)

14. Since we are not trying to simulate systematic errors, there will be some items listed explicitly or implicitly in Appendix A which we will ignore. For example, item 10.B.V., oscilloscope calibration, may be done by recording a square wave of known amplitude and known duration on every oscilloscope photograph immediately before recording the signal. Alternatively, a "staircase" step wave of known values may be used, or a combination of DC (direct current, i.e., constant amplitude) level and constant frequency sine wave, or other calibration signal. Any of these techniques can involve random fluctuation in the amplitude of voltage from the calibration generator (though hopefully not too much if the generator is of the quality one would expect for a calibration source). We propose to include this random error in our simulation. On the other hand, the power supply, say a battery, of the calibration generator could begin to fail. If this were not noticed the operator might set a switch for 100 millivolts but the generator might then actually deliver only about 50 millivolts to the oscilloscope. Such a situation, permitted to persist over a considerable

series of recordings, could provide a serious systematic error. We do not propose to include this kind of error in the simulation.

15. Let's look more closely at the random error in an oscilloscope calibration signal. Let us suppose that we are being very careful and are using an external calibration source instead of relying entirely upon the oscilloscope's sensitivity knob settings. For example, consider the square wave calibration, as in the figure:

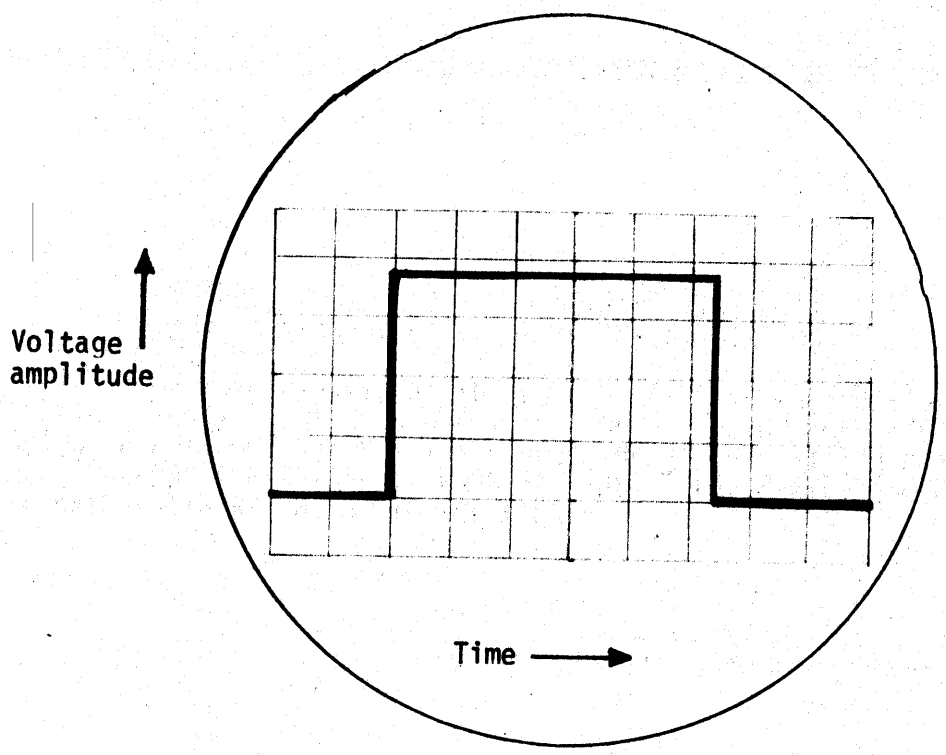

Figure 5.

Let V_0 be the voltage and T_0 the pulse duration which is expected from the calibrator. Then the vertical sensitivity used in the data reduction process as a result of the photograph of this calibration will be about $\frac{V_0 \text{ volts}}{3\frac{3}{4} \text{ centimeters}} = \frac{4V_0}{15} \frac{v}{cm}$. The horizontal sensitivity used would be about $\frac{T_0 \text{ seconds}}{5\frac{1}{3} \text{ centimeters}} = \frac{3T_0}{16} \frac{sec}{cm}$. However, due to random error in the calibrator (or in the instrument which we are using to independently measure the output of the calibrator) there is actually some distribution associated with V_0

and another with T_0. Figure 6 shows the pulse redrawn in a standard Cartesian coordinate system, with the distributions indicated.

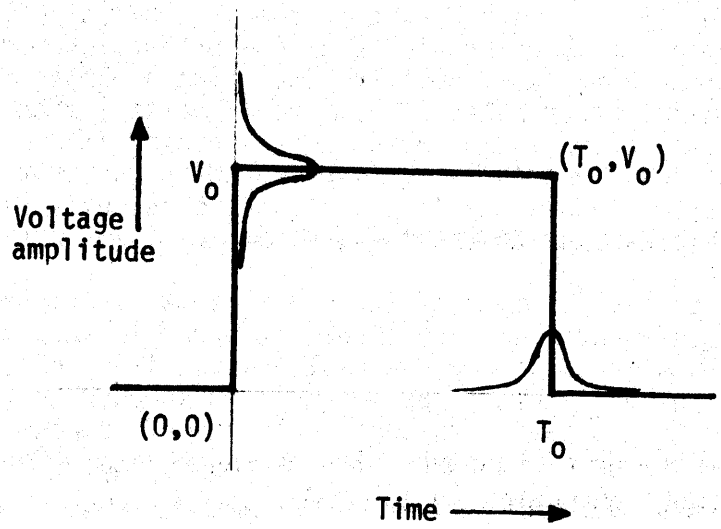

Figure 6.

We don't know what the forms of these two distributions are, let alone the values of their parameters. (In fact we are assuming, so far without proof, that the "wideness" of the distributions is linearly proportional to the magnitudes of V_0 and T_0, where the linear proportionality function has positive slope and passes through the origin.)

16. When this calibration pulse has been photographed, the next step is to put the signal into the oscilloscope and photograph it, preferably on the same piece of film as, and superimposed on, the calibration pulse. Then the photograph might look something like Figure 7.

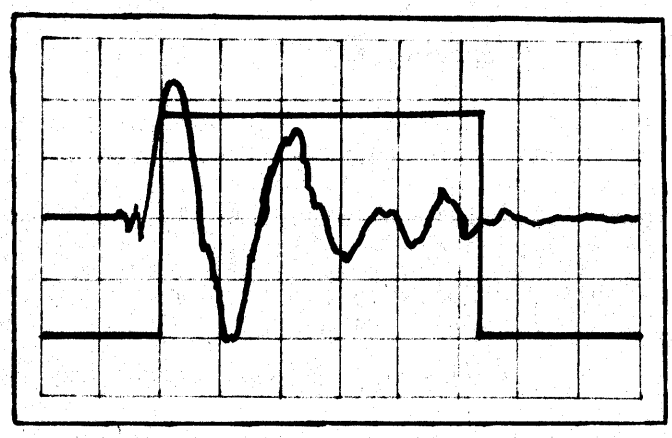

Figure 7.

Part of the data reduction procedure would then be to digitize the calibration pulse, say at its corners. Because of problems such as 10.B.VI., 10.C.II., and 11.B.III.b. in Appendix A, the person (or machine) doing the digitizing might have a hard time deciding precisely which point on the photograph represents the exact corner of the pulse. Then, when he has selected a point, because of haste in a production mode of operation he quite commonly fails to digitize the point he selected, but rather records the digital coordinates of some other point (which is, however, hopefully, quite close to the point he was aiming at). Then the digitization process itself inherently involves rounding (or truncation) error. The three errors cited in the last three sentences effectively serve to widen the distributions shown in Figure 6.

17. The next step is to try to digitize the signal shown in Figure 7. Actually, Figure 7 is somewhat idealized since, in order to keep the trace visible where its slope has large absolute value, it is often necessary to increase the oscilloscope beam intensity so much that the photograph trace exhibits noticeable "blooming" (again cf. Appendix A, 10.C.II. and 11.B.III.b.) where the trace slope is near zero. Thus the signal trace locally might look more like Figure 8.

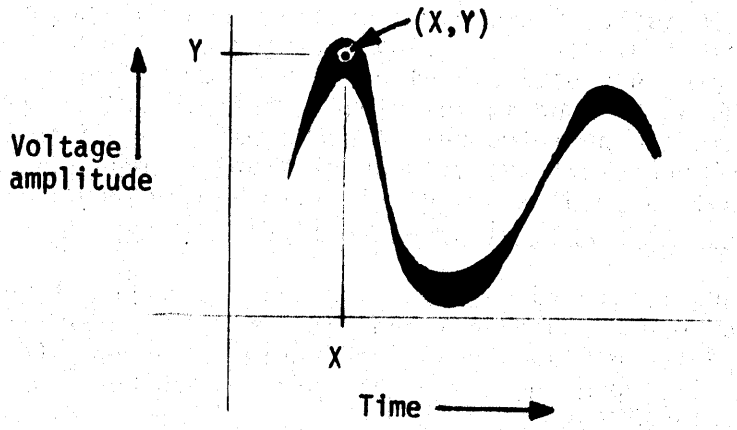

Figure 8.

Thus the three error sources discussed in paragraph 16, above, all apply to digitizing the signal, too. Consequently there are distributions on the digitization of the coordinates of any point, say (X,Y) in Figure 8, also. This uncertainty is indicated in Figure 9.

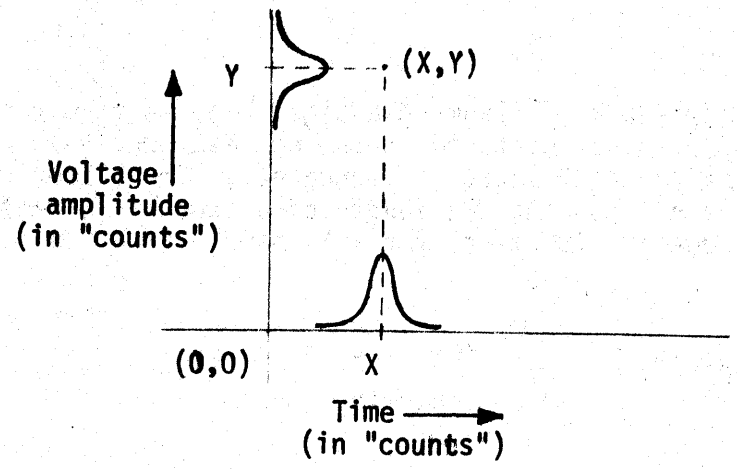

Figure 9.

18. Digitization yields integer numbers of "counts" for the x and y coordinates of the point being digitized, where a "count" is some (hopefully small) fraction of a centimeter and is determined by the kind of digitizer being used. Let X_0 and Y_0 be these two numbers for the point (T_0,V_0) on the calibration pulse in Figure 5, and let X and Y be these two numbers for the point (T,V) in Figure 9. Then the formulas for determining T and V are

$$T = (X \text{ counts}) * \frac{(T_0 \text{ seconds})}{(X_0 \text{ counts})} \qquad (6)$$

and

$$V = (Y \text{ counts}) * \frac{(V_0 \text{ volts})}{(Y_0 \text{ counts})} \qquad (7) .$$

We have seen that all of the quantities V_0, T_0, X_0, Y_0, X, and Y in these two equations have errors associated with them. So the T and V which we calculate for any point in the signal trace will also be in error. The next question is, how great will this error be? There are at least two ways to approach the answer to this question. One is to study and assess individually the three kinds of errors discussed in paragraph 16, above, and determine how they interact for each of the variables X_0, Y_0, X, and Y and how working through these variables they affect T and V (cf. also Appendix B). Error in T_0 and V_0 would also have to be estimated and accounted for. We will illustrate this approach by devoting a paragraph to examining paragraph 16's third kind of error in more detail.

19. (The analytical approach.) Assume the digitizing machine records the integer number of "counts", or distance units, nearest the truth. (That is, assume the machine rounds instead of truncates.) Then, modulus the quantum step length, i.e., modulus the length of a "count" in centimeters, the pdf (probability density function) for this single error is

$$\text{pdf}(x) = \begin{cases} 1 & \text{for } -\frac{1}{2} \leq x < \frac{1}{2} \\ 0 & \text{otherwise} \end{cases}$$

as shown in Figure 10.

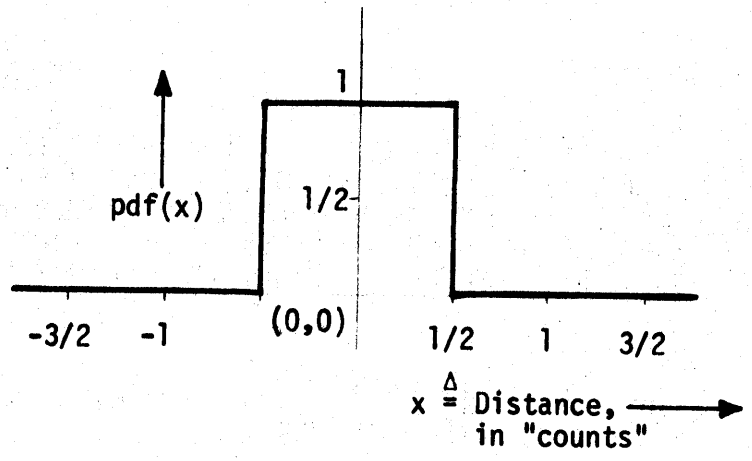

Figure 10.

The mean of this "boxcar" distribution is

$$\mu_x = 0$$

and the variance is

$$\sigma_x^2 = \int_{-\infty}^{\infty} (x-\mu_x)^2 \, \text{pdf}(x) \, dx = \int_{-\frac{1}{2}}^{\frac{1}{2}} x^2 \, dx = \frac{1}{12}$$

Therefore $\sigma_x = \frac{1}{12} = .085$ digitizer "counts". For a digitizer which reads 0 counts at the bottom grid line of the oscilloscope reticle and about 100

counts at the top line, then, the standard deviation of vertical error due to digitization alone, for each point read on both the calibration and signal traces, is about .085% of full scale deflection. Consider the case of a signal which is expected to have approximately zero integral (i.e., have approximately equal amounts of positive and negative variation, as in Figure 7). In this case the oscilloscope would usually be set so that zero signal amplitude is at the center grid line. Also, it is common practice to choose an oscilloscope sensitivity such that the greatest signal variations expected will use about 75% of available full scale vertical deflection. This is done in order to reduce errors from such sources as 10.B.III. and 10.D.II. in Appendix A, and also to leave some margin for unexpectedly large signals. Under these circumstances the maximum expected positive signal would drive the beam about 75% of 3 centimeters above the center line and the maximum negative signal a similar amount below center. Therefore the error under discussion here would have a standard deviation of about

$$\frac{.085 \text{ counts}}{100 \text{ counts} * \frac{1}{2} * .75} * 100\% \doteq .227\%$$

of maximum signal. Put another way, this error would be a source of noise some 53 dB below maximum signal. Noise at this level would be distorting *both* Y *and* Y_0 in equation (7), so it would be the cumulative effect which would be distorting V. (Of course the noise is depressed more if a digitizer is being used which has more than 100 counts for zero to full scale deflection.) When signal is below its maximum level, as it actually is during most of the recording, the signal to noise ratio (due to this one error source) is correspondingly worse since this noise level is constant regardless of signal level. The other error (or noise) sources can only make the signal to noise ratio worse at all signal levels.

20. Paragraph 19 deals only with error source 13.D. in Appendix A. Items 10 through 14, inclusive, in Appendix A have 44 lines of such error sources, and the list isn't complete. Performing an analysis such as that in paragraph 19 for that many sources, for each of the variables on the right hand sides of equations (6) and (7), figuring out how to combine these errors correctly (they are not all independent), and then figuring out how to program the computer to simulate this, not only seems a very tedious undertaking but also seems likely to be fraught with much likelihood of mistake. In paragraph 18 we mentioned that there is a second way to approach the problem. That approach is, we think, quite a bit more feasible than the approach illustrated in paragraph 19, at least for some of the sources of error listed in Appendix A. We proceed now to illustrate the second approach.

21. (The statistical approach.) First, we hypothesize that time random errors from the error sources of interest can be "lumped in" with amplitude errors, as follows. Let Figure 11 represent the cumulative errors on T and V from all the sources represented in Figures 6 and 9 operating through equations (6) and (7).

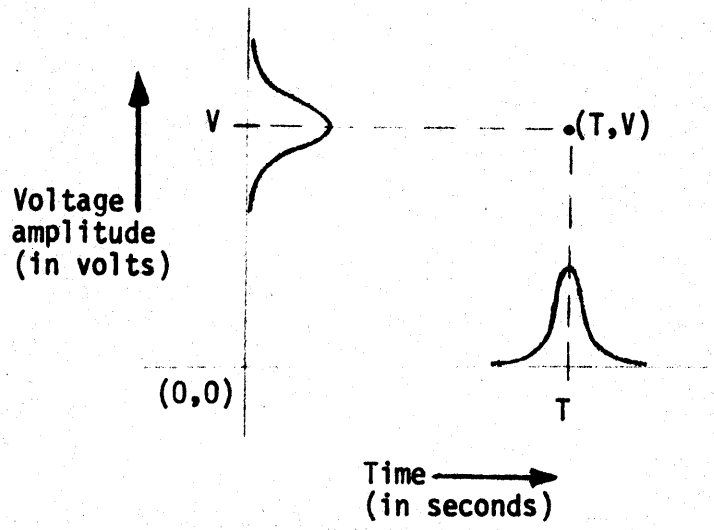

Figure 11.

It is all the more true that we know neither the forms of these cumulative distributions in Figure 11 nor the values of their parameters. Nevertheless, let us proceed. Let ΔT be the error actually committed in the horizontal time scale in trying to record and digitize the particular point (T,V) in Figure 11. Although neither the value of ΔT for this particular point nor its general distribution are known, we do know that the physical function which we are trying to record and digitize has *some* value at the time $T+\Delta T$ at which we have mistakenly taken our reading. Let this unknown exactly correct functional value be denoted by $V(T+\Delta T)$. Let ΔV be the unknown error in the recording and digitization of V, so that the recording and digitization has actually left us with vertical coordinate $V+\Delta V$. (Either or both of ΔT and ΔV may be negative, of course.) To summarize, we tried to record and digitize the coordinates of the point (T,V) but the two unknown error distributions in Figure 11 led us instead to digitize $(T+\Delta T, V+\Delta V)$. Both these two coordinates have error in them. However, the point $(T+\Delta T, V(T+\Delta T))$ is actually on the curve and so, even though it is not the point we intended to record and digitize, *neither* of these two coordinates has *any* error. So let us compare our recorded and digitized coordinates $(T+\Delta T, V+\Delta V)$ not with the coordinates of the point (T,V) which we were aiming at but rather with those of a wholly new point on the curve, $(T+\Delta T, V(T+\Delta T))$. Doing this makes our first recorded and digitized coordinate exact, leaving all the error in the second coordinate. Consequently Figure 11 can now have the error distribution entirely erased from the T coordinate and the distribution function on the V coordinate replaced by some new, still unknown distribution which somehow incorporates both of the old distributions. Plotting the recorded and digitized versions of the numerous points (T_i, V_i), each with its new purely vertical error distribution (still unknown) yields Figure 12.

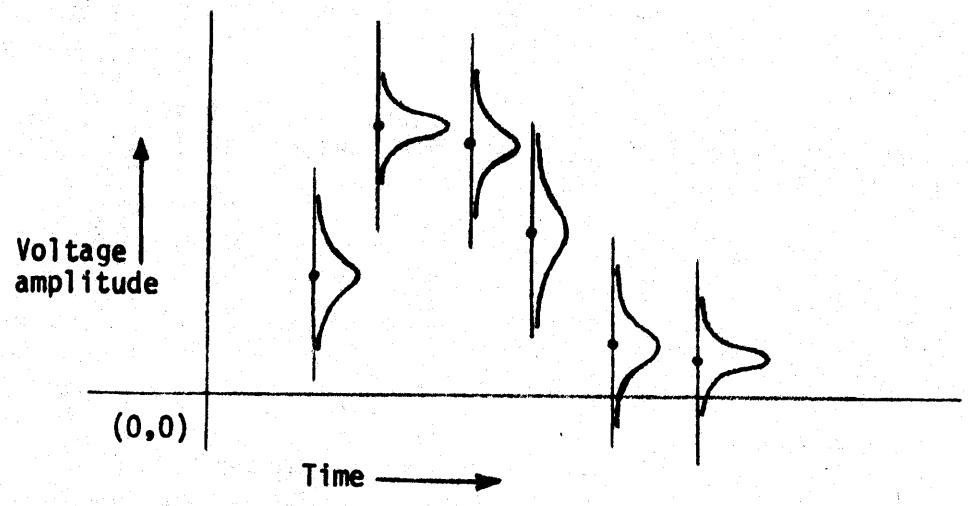

Figure 12.

22. Second, we try to estimate the distributions of these new "lumped" amplitude errors shown in Figure 12. Paragraphs 22 through 31 are devoted to this. We begin by attempting to determine what kind of distribution we have to deal with. We know that the distribution contains the effects of error contributed by numerous sources, e.g., at least those sources numbered 10 through 14, inclusive, in Appendix A (cf. paragraph 13, above). This being so we might be tempted to conclude from the kind of thinking discussed in Appendix B that the distribution was normal. Such a conclusion should be accepted only as an hypothesis, however, unless and until it is confirmed by experiment. We could determine experimentally whether this particular hypothesis was valid by using statistical goodness of fit tests for normality on real data. This has in fact been done. The conclusion of the determination was, "The digitization errors ... show good evidence of normal distribution, with about 80% of the intervals passing the chi-square test at the .05 level of significance. ... we conclude that the vertical digitization errors are normally distributed."[8]

23. Granting therefore that the distributions in Figure 12 are normal, the next task is to determine values for the distribution parameters. The normal distribution has two parameters, viz., mean μ and variance σ^2 (or standard deviation σ). Let us consider first the mean μ. It is not unreasonable to suppose that the mean of the distribution of the digitized value of the vertical coordinate of the pair $(T+\Delta T, V+\Delta V)$ will in general be $V(T+\Delta T)$ (cf. paragraph 21, above; the horizontal coordinate of course then contains no error at all), considering among other things that the normal distribution is symmetric. The error distance between the digitized value $V+\Delta V$ and the mean of the distribution of this value is therefore $|(V+\Delta V)-V(T+\Delta T)|$. This same expression also of course gives the distance from the digitized value to the accurate value of the data at time $T+\Delta T$. Therefore the distribution of the accurate value about the digitized value is the same as the distribution of the digitized value about the accurate value, except that the mean of the former is $V+\Delta V$ instead of $V(T+\Delta T)$. Consequently we may take the dots in Figure 12 as the digitized values $V+\Delta V$ and the distributions in the figure

as representing the likelihood that the accurate value $V(T+\Delta T)$ is within a specified vertical distance of that digitized value. That is, the mean of the distribution of $V(T+\Delta T)$ is

$$\mu = V + \Delta V \qquad (8) .$$

24. The next consideration is, what is the standard deviation σ of the normal (cf. paragraph 22, above) distributions shown in Figure 12? σ gives an indication of the "wideness" of a distribution. Put another way, large values of σ indicate that the error in a vertical digitization reading is likely to be large. We may begin our estimation of the value of σ, therefore, by observing that, whatever the error in recording and digitizing $V(T+\Delta T)$ may be, we would expect that it would in general be greater where the signal had a slope with great absolute value than where the slope was near zero. (Notice that the distributions in Figure 12 were drawn to conform with this observation.) To see this, let m denote the average slope of the function from (T,V) to $(T+\Delta T, V(T+\Delta T))$. That is,

$$m \triangleq \frac{V(T+\Delta T) - V}{(T+\Delta T)-T} \equiv \frac{V(T+\Delta T) - V}{\Delta T} .$$

From this definition it follows immediately that

$$V(T+\Delta T) - V = m * \Delta T \qquad (9) .$$

But the left hand side of this equation is just the discrepancy between $V(T+\Delta T)$ and the vertical coordinate of the point *which the digitizer was aiming at*. If his aim was fairly good, then the left hand side is very nearly the cumulative ("lumped") random error in the digitized value of $V(T+\Delta T)$. In any case the left hand side should be the mean of the distribution of that error. And the left hand side of equation (9), being equal to the right hand side, is directly proportional to the function slope m. Therefore large function slope should generally produce large combined (i.e., cumulative, or "lumped", in the sense of paragraph 21) error in recording and digitizing $V(T+\Delta T)$, for a given error ΔT in digitizing T.

25. To understand the standard deviation of the cumulative ("lumped") error distributions shown in Figure 12 in more detail, however, we must take account also of the fact that, for a constant setting of the oscilloscope beam intensity control, the tracewidth (and therefore the size of the target which

the digitizer has to aim at) decreases as the oscilloscope beam traversal speed increases. Oscilloscope companies try to make the output of the horizontal sweep generator as linear as possible, so the horizontal component of the beam speed is roughly constant. Consequently the beam speed increases as the direction of travel departs from the horizontal. To quantify this speed increase, consider Figure 13.

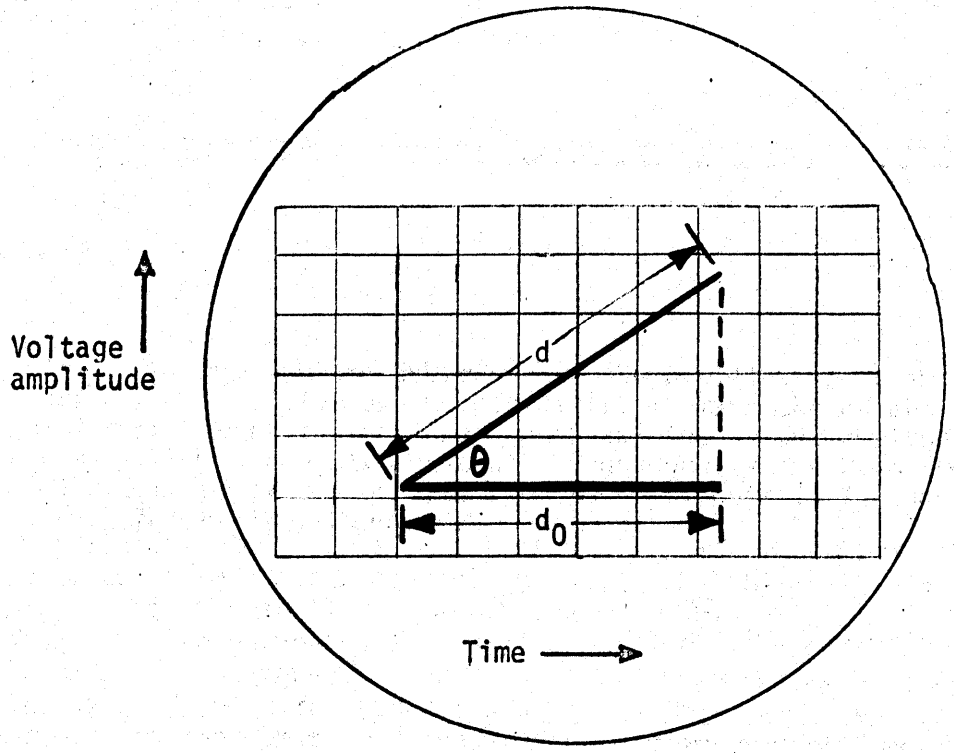

Figure 13.

In this figure d_0 is the horizontal distance which the beam would travel in time duration δt, and d is the distance the beam actually travels in that same amount of time when the trace makes an angle θ with the horizontal. For small time lapses δt, then, the horizontal beam speed is $s_0 \overset{\Delta}{=} d_0/\delta t$ and the instantaneous speed is $s \overset{\Delta}{=} d/\delta t$. From the figure,

$$\cos\theta = \frac{d_0}{d} = \frac{d_0/\delta t}{d/\delta t} \equiv \frac{s_0}{s} \Longrightarrow$$

$$\Longrightarrow \quad s = \frac{s_0}{\cos\theta} = s_0 \sec\theta \qquad (10) .$$

Just how does this instantaneous beam speed affect the size of the target which the digitizer is aiming at, and his accuracy in hitting that target? Consider a magnified view of the trace, as shown in Figure 14.

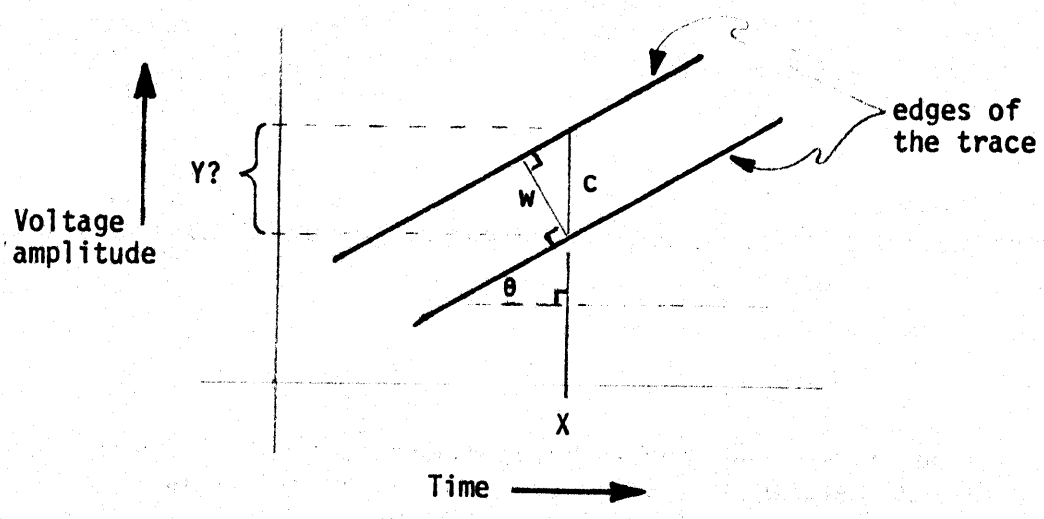

Figure 14.

The figure shows that w is the (non-negative) width of the trace and θ is its angle with respect to the (horizontal) time axis. From inspection of the figure we would expect that the error in choosing the exact vertical coordinate Y to associate with time coordinate X will be directly related to the vertical sectional width of the trace. In other words, what point along the line segment (vertical cross section) of length c in Figure 14 should the digitizer choose for the Y to correspond with the X in the figure? Especially if the trace happens to be bending the answer need not be simply "the center of the segment". In any event experience has shown that a person operating a digitizing machine in a production mode will often be satisfied with any point along that segment. So we repeat, we would expect that the error in Y would be related directly to c. Can we find a functional relationship between c and some simple observables of the data, perhaps for example the local trace slope? From Figure 14 we see that

$$\cos\theta = \frac{w}{c} \Longrightarrow$$

$$\Longrightarrow \quad c = \frac{w}{\cos\theta} = w \sec\theta \qquad (11) .$$

Consequently, to get a function to predict c we will need a model for the behavior of tracewidth w. Let us consider two such models, then choose one of them.

26. (First model: constant area per unit time.) In both of the two models we will assume that the total amount of energy falling on the whole oscilloscope face, and subsequently on the film, per unit time is constant. In the first model we will assume in addition that the spatial distribution of the energy is such that the area of film exposed per unit time is also constant. Figure 15 shows a segment of the trace as exposed on the film during time segment δt.

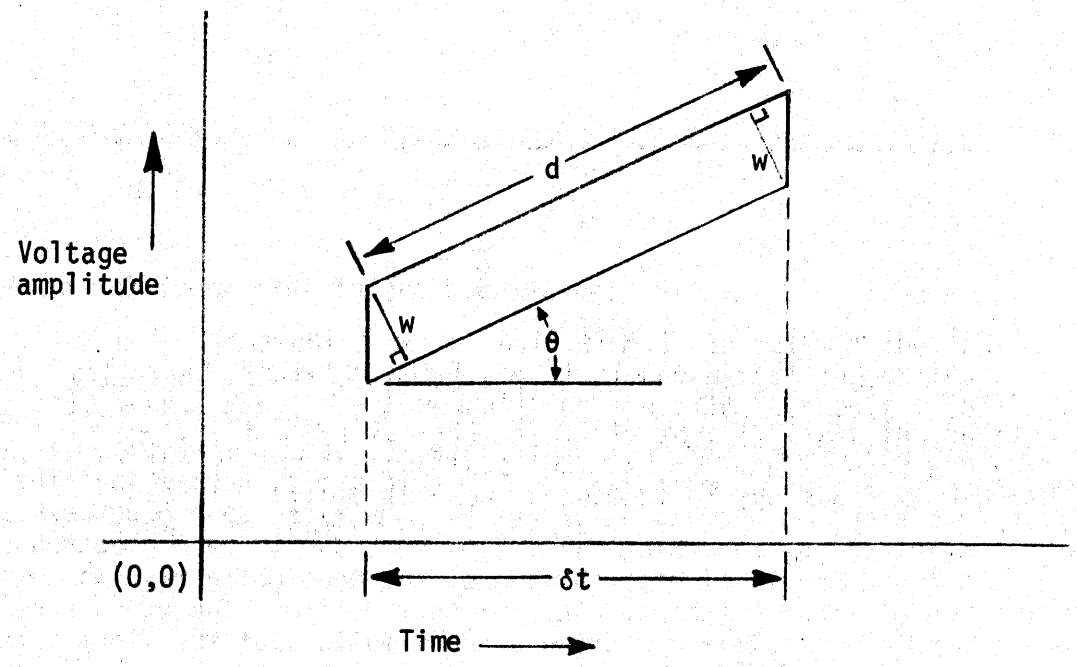

Figure 15.

The trace segment has the shape of a parallelogram if δt is not too great, so the area of the segment is $w*d$. By assumption this area is constant for fixed δt, so define

$$C_1 \triangleq w * d \qquad (12) .$$

From the figure, $\cos\theta = \frac{\delta t}{d} \Longrightarrow d = \frac{\delta t}{\cos\theta} = \delta t \sec\theta$. Putting this into equation (12) yields

$$C_1 = w * \delta t * \sec\theta \Longrightarrow w \sec\theta = \frac{C_1}{\delta t} .$$

Since this discussion is for fixed δt (say a unit amount of time), we can define a new constant $C_2 \triangleq C_1/\delta t$. Then by the last equation

$$w \sec \theta = C_2$$

By equation (11), therefore,

$$c = C_2 \qquad (13)$$

(cf. Figure 14). That is, the two assumptions of this model for tracewidth behavior imply that c is a constant.

27. (Second model: normal cross sectional distribution of energy.) In the second model of tracewidth behavior we will still accept the first assumption in paragraph 26, above, but we will replace the second assumption in that paragraph with a more complicated one. Specifically, assume that the oscilloscope electron beam is at any given time aimed to produce exposure at a single point on the recording film. However, due to beam electron scatter there is a two dimensional distribution of the beam which results in a distribution of light intensity incident on the film. The cross section, taken perpendicular to the direction of beam motion, of the light intensity distribution is normal. The magnitude of the local intensity is inversely proportional to the speed of the beam as it sweeps past. The film-phosphor combination has no memory, i.e., the incident light intensity is sensed instantaneously, not cumulatively. Finally, the film-phosphor combination is binary, in the sense that there is a characteristic constant threshhold such that if the electron beam intensity surpasses this threshhold level the film is, at that point, completely exposed; otherwise the film remains unexposed. (This threshhold value is a function of numerous things, such as film speed, but is constant over the entire area of a single data photograph.) Under this assumption the energy falling on the film will expose it wherever the energy density is great enough, but out at the "tails" of the normal distribution the film will remain unexposed because the energy intensity there will have fallen below the film exposure threshhold. Figure 16 shows a cross section (perpendicular to the direction of beam travel) of the instantaneous light intensity, compared to the film exposure threshhold level.

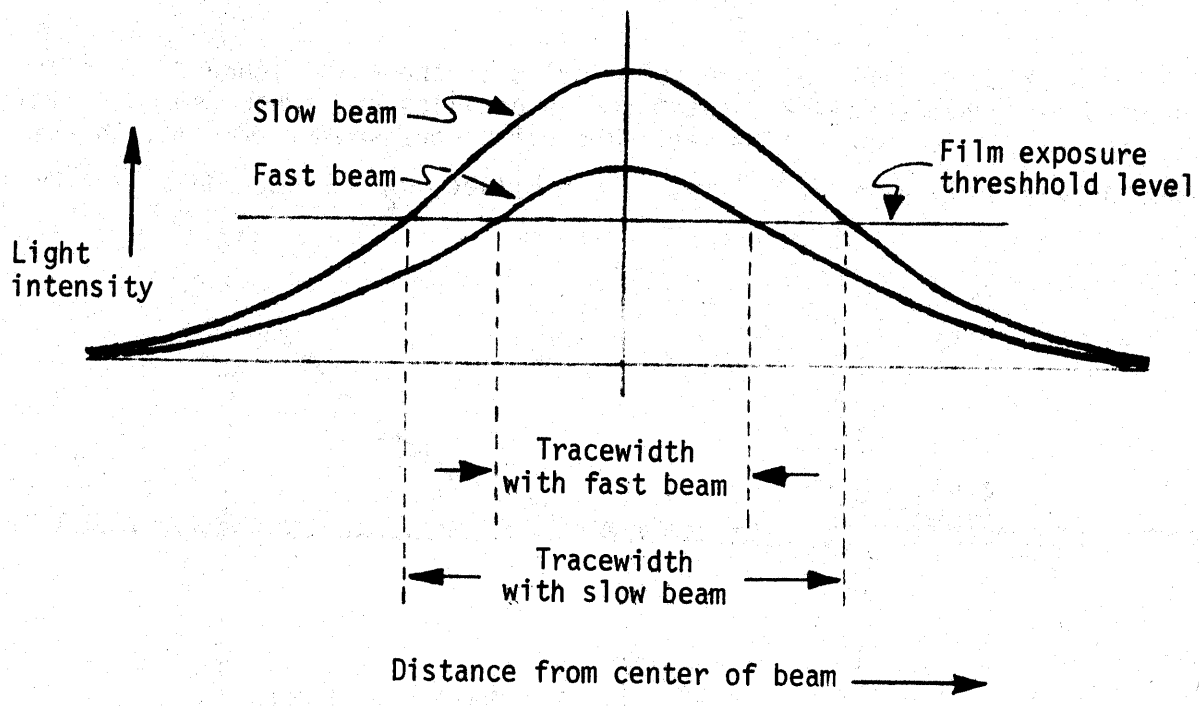

Figure 16.

The slow beam is intended to be represented in this figure as traversing at two thirds the speed of the fast beam, so that the slow beam is depositing one and a half times as much energy per unit area per unit time as is the fast beam. Of course, the beam of an oscilloscope traverses at its lowest speed when it is travelling horizontally across the face of the tube, i.e., at speed s_0 (cf. equation (10)). Therefore the instantaneous intensity of the passing beam, under this model, normalized to the intensity when the beam is traversing horizontally, is given by the first expression in Appendix C. There are two variables in this expression, viz., s, the instantaneous beam speed, and w, the perpendicularly cross sectional width of the trace recorded on the film. The quantity $\tilde{\sigma}$, the standard deviation of the normal distribution of the intensity, may be eliminated by first noting that at the edge of the recorded trace the exposing intensity must be precisely the postulated threshhold intensity I_0. So we set the intensity expression, evaluated at two different beam speeds s_1 and s_2, with x given the corresponding values $w_1/2$ and $w_2/2$ of distance from the beam or trace center to the trace edge (where $I = I_0$), equal to itself. From this point the derivation in Appendix C is straightforward. It concludes by presenting the vertical cross section c of the trace as a function of s and various constants peculiar to the individual data recording photograph. Applying equation (10), the final equation in Appendix C becomes

$$c = (\sec\theta)\sqrt{w_1^2 - \frac{w_2^2 - w_1^2}{\ell n \frac{s_1}{s_2}} \ell n \frac{s_0 \sec\theta}{s_1}} \qquad (14)$$

or else, should the radicand become negative, $c = 0$. The general shape of

this function of (the absolute value of) θ is shown in Figure 17. (This particular example was calculated for an oscilloscope sweep "speed" setting of 10 ns/cm, i.e., s_0 = 1 Mm/sec. The other constants taken from the particular photograph trace were w_1 = 1 mm, s_1 = 5 Mm/sec, w_2 = 2 mm, and s_2 = 2 Mm/sec.)

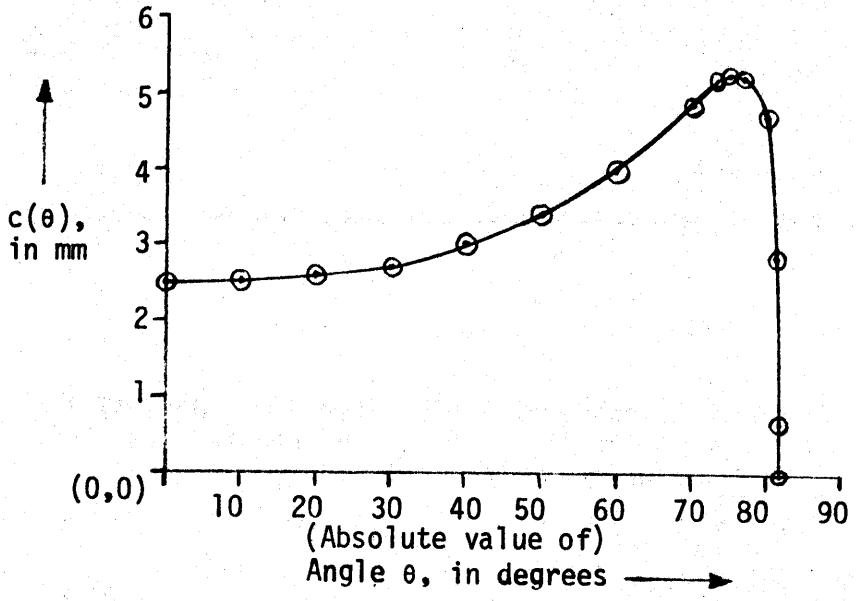

Figure 17.

28. In the preceding two paragraphs we have considered two models for tracewidth behavior. From each we have deduced a functional relationship between c and θ (cf. Figure 14). Which model are we to believe? Fortunately there is a very simple way of choosing between these two models. In the second model (that of paragraph 27) there is a finite instantaneous beam traversal speed (and therefore a $\theta_0 < \frac{\pi}{2}$) at which the tracewidth w will become 0, i.e., the trace will vanish. This can be seen intuitively by examining Figure 16: when the distribution drops entirely below the film exposure threshhold level, then w becomes zero. It also follows analytically from equation (14), since the radicand will become zero when

$$w_1^2 = \frac{w_2^2 - w_1^2}{\ell n \frac{s_1}{s_2}} \ell n \frac{s_0 \sec \theta_0}{s_1} \quad \Longleftrightarrow$$

$$\Longleftrightarrow \quad \frac{s_1}{s_0} e^{\frac{w_1^2 \ell n \frac{s_1}{s_2}}{w_2^2 - w_1^2}} = \sec \theta_0 \quad \Longleftrightarrow$$

$$\Longleftrightarrow \quad \cos\theta_0 = \frac{s_0}{s_1} e^{-\frac{w_1^2 \ln \frac{s_1}{s_2}}{w_2^2 - w_1^2}} \quad \Longleftrightarrow$$

$$\Longleftrightarrow \quad \theta_0 = \cos^{-1}\left(\frac{s_0}{s_1} e^{-\frac{w_1^2 \ln \frac{s_1}{s_2}}{w_2^2 - w_1^2}}\right) \qquad (15) .$$

For the parameter values associated with Figure 17, for example, according to the second model the trace should vanish entirely at $\theta_0 = 81.526°$. On the other hand, in the first model (that of paragraph 26) the trace can never entirely disappear (cf. equation (13)). Yet we know that in real life the trace *can* disappear entirely when θ becomes sufficiently great.[9] Therefore we choose the second model, despite the relative simplicity of the first. -- -- Of course, we could construct yet other models for tracewidth behavior than just these two. However, the authors of this paper have in their investigations of these matters come to believe that the second model presented here is adequately realistic and yet simple enough for purposes of estimating errors in calculating transfer functions from pulse data. In the following discussion we will introduce experimental evidence which supports this belief.

29. Let us now pause for a moment to summarize where we stand with respect to the question which we raised at the beginning of paragraph 24, viz., what is the standard deviation σ of the normal (cf. paragraph 22, above) distributions shown in Figure 12? Our analysis has indicated that σ is a monotone increasing function of both the absolute value of the local trace slope m (paragraph 24) and the local vertical cross section c of the trace (paragraph 25). In paragraphs 26 and 27 we developed models for the vertical cross section of the trace, and in paragraph 28 we presented an argument for selecting the model represented by equation (14). The question now is, precisely what function of $|m|$ and c is σ ?

30. To get an insight into this question, consider a redrawn version of the type of information shown in Figure 17, in which c is the horizontal axis (instead of the vertical) and the vertical axis is absolute value of slope m (i.e., of tan θ instead of angle θ). Figure 18 shows the new drawing. (The reason for portraying c in this new way is to facilitate comparison of our theory with some previously published experimental data, as promised at the end of paragraph 28. Also, rather than just mechanically reproducing Figure 17 in a new coordinate system we have, in order to use the new figure to convey as much new information as possible, used new parameter values in Figure 18. This particular example was calculated for an oscilloscope sweep "speed" setting of 10 ns/cm, i.e., $s_0 = 1$ Mm/sec, as before, but the other constants taken from the particular photograph trace were $w_1 = 1$ mm, $s_1 = 1$ Mm/sec, $w_2 = .8$ mm, and $s_2 = 2$ Mm/sec.)

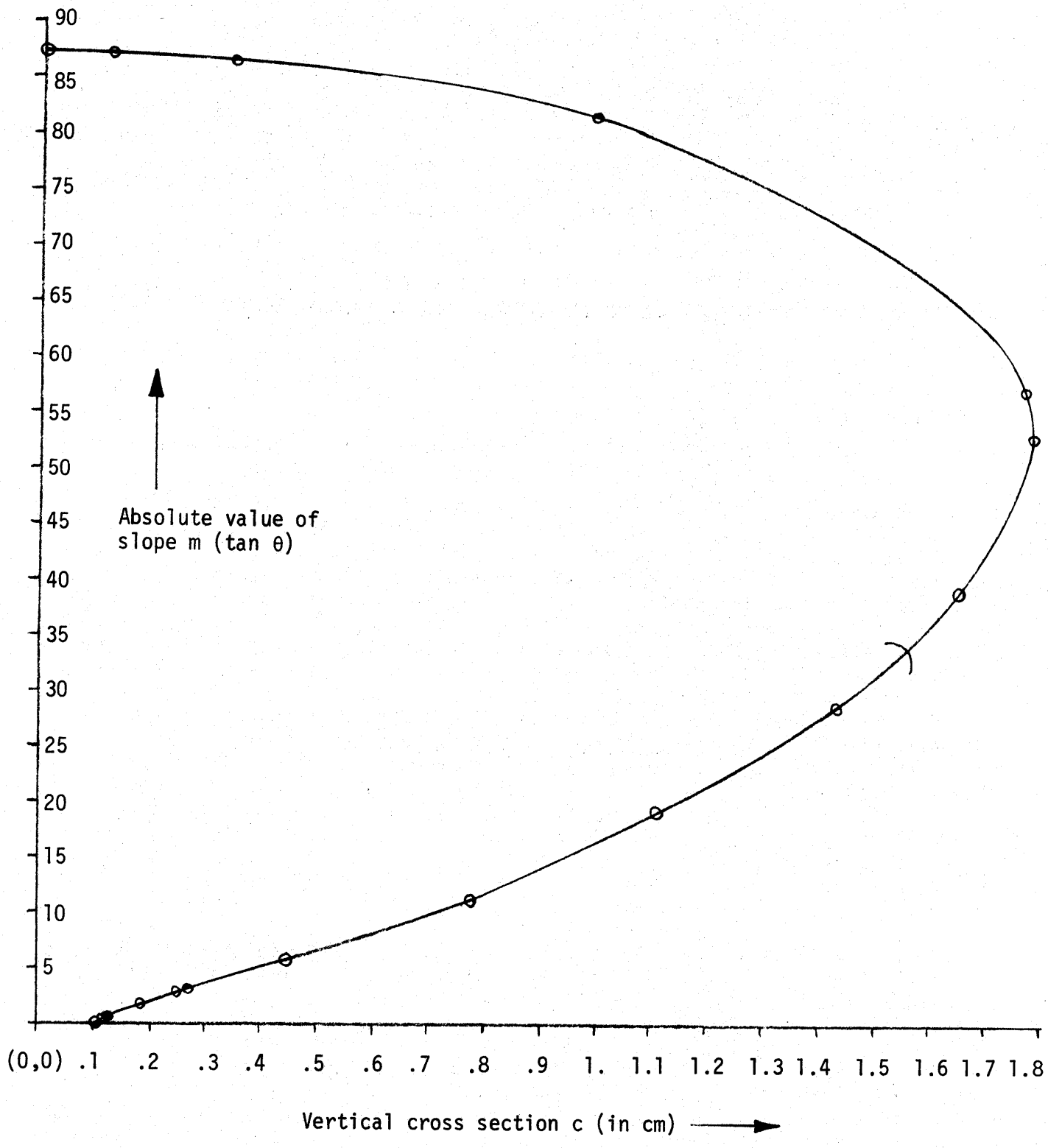
90
85
80
75
70
65
60
55
50
45
40
35
30
25
20
15
10
5
Absolute value of
slope m (tan θ)
(0,0) .1 .2 .3 .4 .5 .6 .7 .8 .9 1. 1.1 1.2 1.3 1.4 1.5 1.6 1.7 1.8
Vertical cross section c (in cm)

Figure 18.

Figure 18 shows that, for the particular data photograph from which it was constructed, according to the model of paragraph 27 the trace will remain visible except where the data drives it to a slope of absolute value greater than about 87.5 (cf. equation (15)). The figure also shows that the model predicts the vertical cross section of the trace on this particular data photograph should increase until the slope reaches about 53. (The exact peak can of course be found by setting the derivative with respect to θ of the right hand side of equation (14) equal to zero and then solving for θ.) Now, ordinarily oscilloscope controls would not be set so that anticipated data would produce absolute values of slope in excess of such extremes. Even if the data were to contain unexpectedly high frequency content, so that the data trace did exhibit slopes of absolute values greater than these, people operating digitizing machines would not, ordinarily, choose these places in the data to digitize: it is much more common to choose critical points ("corners") on the trace for taking digitization readings.[10] Therefore our interest in Figure 18 is primarily up to the general part of the curve upon which the "close parenthesis" has been superimposed in that figure. We are not saying validity of the model is restricted to the lower portion of the curve, but only that that is the portion of the model which we would expect to use most often with real, carefully recorded and digitized data. In this portion of the model $|m|$ and c increase together. Therefore in this portion of the model a function which increased with c would also increase with $|m|$, and vice versa. The question is still, what function of $|m|$ and c is σ ? The simplest approximation we might make, in view of the foregoing, therefore, is that σ is simply a scalar multiple of $|m|$ or of c.[11] Assuming for a moment that the function really is this simple, we must then ask, *what* scalar multiple? There are several ways to attack this question. One direct way is to conduct the experiment of studying real data to see what function σ really is of $|m|$ or of c. At least part of this experiment has in fact been performed. Figure 19 is a photo-reproduction of a figure in the published report of that experiment.[12] This figure shows that σ is indeed a fairly linear function of $|m|$, within the experimental error of the procedures used to produce the figure, at least for small values of $|m|$. Therefore this experimental data corroborates our guess that σ is simply a multiple of $|m|$ or of c. This being so, we might be tempted to say immediately that $\sigma = k_1 * |m|$, and devote ourselves from here forward to trying to discover the value of k_1. However, there is also the possibility that $\sigma = k_2 * c$. In the region of Figure 18 below the parenthesis the forms of these two equations of σ would be much the same. But for values of $|m|$ above about 35 the two equations would begin to disagree sharply. Which, then, are we to accept? The hypothesis $\sigma = k_1 * |m|$ is to be rejected, for two reasons. First, Figure 19 shows that, contrary to the prediction of this hypothesis, σ is appreciably different from zero when $|m| = 0$. (This is not surprising, since the tracewidth is large when $|m| = 0$: cf. Appendix A, 10.C.II.) For the second reason, look again at paragraph 24. Equation (9) implies that the vertical error increases linearly with $|m|$ *provided* ΔT *is constant. But the error* ΔT *should become less and less* when $|m|$ becomes sufficiently great that the trace becomes an almost vertical, very thin line. Consequently the vertical error, the left hand side of equation (9), is not a linear function of $|m|$ for large values of $|m|$. (Besides, our experience with people operating digitizing machines indicates that, in those rare instances when the operator

2.1E+07
1.4E+07
7.0E+06
0.
-7.0E+06
-1.4E+07
-2.1E+07
DFDT
0.
3.0E-03
6.0E-03
9.0E-03
1.2E-02
1.5E-02
1.8E-02
2.1E-02
2.4E-02
SIGMA

Figure 19.12

elects to try to digitize a point in a portion of the trace with high absolute value, he is unusually careful.[10]) Therefore, we are left with the hypothesis that

$$\sigma = k * c \qquad (16),$$

where $c > 0$. As with any hypothesis about the real world, equation (16) can (and should) be checked by experiment. The experiment in this case would be to measure both σ and c for real data and confirm whether or not their ratio is approximately constant, at least for significant sets of data (e.g., all the data on any single oscilloscope photograph). Unfortunately this experiment has not yet been performed, so far as the authors are aware. However, the experimental data presented in Figure 19 is relevant, and can be used to argue qualitatively[13] that equation (16) is an acceptable hypothesis pending further, more quantitative, evidence. Equation (16) agrees qualitatively with the data shown in Figure 19 in four ways. First, they both give the reasonable result that the value of σ is greater than zero when the slope of the trace is zero (cf. equation (14)). Second, in both cases the value of σ initially increases as the absolute value of the slope of the trace increases. Third, both give an approximately linear relation between the trace slope absolute value and σ for small values of σ. Fourth, equation (16) results in a plausible way from the digitization process actually used. Therefore this relation will be used in the following treatment.

31. We must now examine more closely the value of k in equation (16). It is the experience of the authors with semi-automatic digitizing in a production mode, involving as it does some pressure to hurry, that taking a digitization reading altogether outside (though usually not very far outside) the boundaries of the trace is not at all uncommon.[10] We nevertheless estimate that some 98% of all readings can be expected to be taken inside the trace boundaries even in a production digitization mode. That is, on a typical data photograph processed in a routine production mode as many as 5 of the digitization readings will actually be taken slightly outside the edges of the trace.[10] 98% of a normal population lies within a trifle less than ±2.33 standard deviations of the population mean. If our estimate of 98% is correct, therefore, the vertical cross section c of the trace is approximately 4.65 standard deviations "long". By equation (16), therefore,

$$k = \frac{\sigma}{c} \doteq \frac{1}{4.65} \doteq .215 \qquad (17).$$

Any other estimate than our 98% could be used to generate a corresponding value of k in this same way. The best estimate of how often a particular kind of digitizing arrangement actually hits the trace is to be obtained from analyzing *real data digitized in a production mode*. We (the authors) are unaware of any estimates of this quantity obtained in this way up to the time of preparation of this paper. Therefore we will use our estimate of 98% in

the example procedure for error estimation to be developed. If and when a better estimate becomes available, however, our illustrative value of k (cf. equation (17)) should be updated accordingly.

32. In paragraph 21 we set out to outline a statistical approach to estimating the data reduction random error from many of the sources and subsources of error listed as items 10. through 14., inclusive, plus item 15.D., in Appendix A (cf. paragraph 13, above). Since then we have developed Figure 12 and equations (8), (14), (16), and (17) to help us in this endeavor. These equations provide us with the means μ_i and the standard deviations σ_i of the normal (cf. paragraph 22) distributions of Y_i in the coordinate pairs (X_i,Y_i) (X_i has no error: cf. paragraph 21) in Figure 12. Consequently we can now produce error bars about the Y_i in either of at least two ways. One way is to graph the set $\{(X_i,Y_i)\}$, then for error bars overlay graphs of, say, $\{(X_i,Y_i+1.645\sigma_i)\}$ and $\{(X_i,Y_i-1.645\sigma_i)\}$. Approximately 90% of a normal population lies within $\pm 1.645\sigma$ of the population mean. Therefore the interpretation of these error bars would be: one could be approximately 90% confident that another digitization of the data would generate a value of Y between these error bars for any randomly selected value of X.

33. The second way of generating error bars for the digitized time domain data is a somewhat more elaborate ruse from order statistics, a ruse which will be useful again in later paragraphs. This second way is as follows. Using μ_i and σ_i we can obtain from a random normal number generator new estimates $\tilde{Y}_i$ of the digitized vertical coordinates.[11] That is, we can get a new set of samples from the distributions shown in Figure 12. The set $\{(X_i,\tilde{Y}_i)\}$ is actually a simulated outcome of applying the given digitizing process to the individual data photograph. We may refer to this set as a pseudo-digitization of the data. These pseudo-digitization values, like the σ_i used in the first error bar scheme (described in paragraph 32, above), will contain simulated error from all the sources in Appendix A of which we took account in constructing the model of paragraph 27. If we pseudo-digitize several times then for each X_i we could use the greatest and least values of $\tilde{Y}_i$ as error bars for the digitization of the (time domain) data. Such error bars can be given a precise interpretation using a "distribution free" interval estimator, such as is provided by Wilks' Tolerance Theorem[14]:

$$C(n,F) = 1 - F^n - n(1-F)F^{n-1}$$

$$= 1 - nF^{n-1} + (n-1)F^n \qquad (18)$$

where n is the number of elements in the sample, F is any fraction between 0 and 1, and C(n,F) is the confidence that at least a fraction F of the population is "trapped" between the largest and the smallest values in the sample. For example, if there are 25 values for $\tilde{Y}_i$ then according to Wilks' Tolerance Theorem our confidence that the greatest and least of the 26 digitization values (1 real and 25 pseudo) "trap" at least 85% of the population between them is

$$C(26,.85) = 1 - .26*(.85)^{25} + 25*(.85)^{26} \doteq 92\%$$

(cf. equation (18)). That is, we may be approximately 92% confident that, for a single randomly selected value of X, at least 85% of an infinite set of future digitizations would produce values between the graphs of $\{X_i,\max\{Y_i\}\}$ and $\{X_i,\min\{Y_i\}\}$, where $\{Y_i\} \triangleq \{\tilde{Y}_i\}\cup\{Y_i\}$. Equivalently, we may be approximately 92% confident that the graph of another real digitization of the entire data photograph would lie between these two error bar graphs for at least 85% of the X values.

34. Paragraphs 32 and 33 offered two ways of estimating the error committed in performance of parts of steps II and III of the procedure outlined in paragraph 8, above (cf. also paragraph 13, above). The next part of step III is to apply a numerical Fourier transform algorithm (assumed correctly programmed) to the actual digitization readings. This should yield a best estimate of the Fourier transform of the recorded data, given the particular digitization of that data and given the particular transform algorithm. We are now in a position to estimate a large part of the error in that estimate. We can put error bars on the magnitude, say, of the calculated transform in either of two ways, quite analogous respectively to the two kinds of error bars described in paragraphs 32 and 33, above. The first way is to derive analytically, from knowing which specific arithmetic operations are used on the normally distributed input random variables by the particular transform algorithm, what must be the distribution of the output of that algorithm. For example, if the algorithm obtains the real and imaginary parts of the transform at each frequency ω by a process which is equivalent to summing products consisting of Y_i times functions of X_i (e.g., $\cos \omega T_i$), i.e., a normally distributed variable times an error free constant (cf. paragraphs 21 and 22, above), then the real and imaginary parts of the calculated transform will be normally distributed.[15,11] If the constants in the sum were such that the means and variances of these latter two normal distributions came out about the same, then the square of the magnitude of the transform, being the sum of the squares of the (normal) real and imaginary parts of the transform, would be chi-square distributed.[16] In that case the magnitude itself would be Maxwell distributed.[17] Since the μ_i and the σ_i are known for all of the original random variables in this chain of functions, the values of the parameters of each of the succeeding distri-

butions in the chain can be calculated by the reader who is interested in looking up and applying each of the footnoted theorems. Error bars could then be put on the magnitude of the numerical Fourier transform using values of the Maxwell distribution parameters in the same way as was done to the time domain data using values of the normal distribution parameters (cf. paragraph 32, above). Similarly, at step IV of the procedure in paragraph 8 it may be decided that the square of the magnitude of the transfer function, being the quotient of the squares of the magnitudes of two numerical transforms (cf. equation (4)), each of which is chi-square distributed, must be Snedecor F distributed.[18] In this way error bars analogous to those of paragraph 32 could also be put on the calculation of the magnitude of the transfer function. Error bars for the calculated phase of both the numerical Fourier transform and the transfer function could be produced in a similar way. -- With these general observations we will here leave any further pursuit in this paper of the details of error bars generated by this kind of statistical analysis.

35. The second way of estimating the error in the calculation of the numerical Fourier transform follows the idea of paragraph 33, above. Applying the numerical Fourier transform algorithm to a pseudo-digitization of the data, i.e., numerically Fourier transforming a set $\{(X_i, \tilde{Y}_i)\}$ (cf. paragraph 33, above), we can obtain from equation (3) a new estimate of the Fourier transform of the given data. For a given frequency ω this new pseudo-transform will generate a point in the complex plane. This complex point, like the point generated at that frequency by the transform of the real digitization of the data, will contain error from all the error sources in Appendix A of which we took account in constructing the model of paragraph 27 plus error from all the sources of random error in the numerical transform algorithm being used (including the error in the interpolation function between digitization points, etc.). Executing procedure step III repeatedly with such pseudo-digitizations as well as with the real digitization will generate at each frequency a family of such complex points. To obtain error bars on the magnitude, say, of the transform we now need only apply Wilks' Tolerance Theorem to the set of magnitudes of these complex points. Cf. equation (18) and the example following it. Error bars can be obtained in the same way from the same family of complex points for the phase of the transform.

36. The error committed in calculation of the transfer function can be estimated by continuing the process advanced in the last paragraph. For each pseudo-transform of the input function f(t) (cf. Figure 1), a pseudo-transform of the output g(t) is used in equation (4) to generate a pseudo-transfer function. For a given frequency ω the set of pseudo-transfer functions will generate a family of complex points containing error from all the sources discussed so far plus that incurred at step IV of the procedure (cf. paragraph 8, above). In the same way as in the last paragraph applying equation (18) to this family of points will yield error bars for the magnitude and phase of the transfer function calculated from the real digitizations of the data.

Part IV. A proposed solution to the problem.

37. The problem which we set out to try to find a way to solve in paragraph 11 was, how may the random error in transfer functions calculated by reducing pulse data be estimated? In Part III of this paper we have considered numerous aspects of that problem. As a result of these considerations we are now able to propose in complete detail an example of a procedure which produces meaningful error bars which incorporate many of the error sources listed in Appendix A. That example appears in Appendix D. As was shown in paragraph 32, the meaning of the error bars generated by the procedure of Appendix D is that one may be approximately 92% confident that any future single reduction of the given, individual piece of data ("from scratch") will generate curves which lie within the bars for at least 85% of the abscissa values. Thus, the error in the reduction of this particular data is estimated, with 92% confidence, to be less than the difference between the reduction values (center line) and the error bars at least 85% of the time.

38. The procedure presented in Appendix D has actually been programmed and made operational in a working, production data reduction mill. Figures 20 through 26 show the result of applying this procedure to two sets of data. The center curve of Figure 20 represents the digitization of the input signal and the two outer curves indicate an estimated ±1.75 standard deviations from the digitization. The boundaries therefore contain approximately 92% of the normal population. Figures 21 and 22 show the magnitude of the Fourier transform of the digitization of the input signal along with the predicted bounds on the error. Note that while the magnitude of the error in the transform does not increase at high frequencies, the relative error increases substantially. Figures 23 through 25 show similar results for the output signal. Figure 26 is a plot of the calculated magnitude of the transfer function and of the associated error bars. It can be seen that in this case the transfer function contains order of magnitude errors over most of the frequency range shown, so that considerable caution would have to be used in drawing conclusions based on this calculation of the transfer function magnitude.

39. In actually using the procedure given in Appendix D it was discovered that the increase in computer time required to numerically Fourier transform not only the digitized data but also many pseudo-digitizations of that data can be quite noticeable. On the other hand, equation (18) makes clear that, using this scheme, it is desirable to transform as many pseudo-digitizations as one can afford to (25 in the example in Appendix D). These two facts together make it clear that it pays in the accuracy of the error estimate to employ the fastest Fourier transform algorithm available (without sacrificing transform accuracy). This being the case we would like to include here a description of a simple device which will greatly increase the speed of most numerical Fourier transform algorithms when they are applied to these pseudo-digitizations. The device is this. Modify the transform program so that when it is calculating the transform using the real digitized values for a piece of data at a particular frequency it *stores* the results of every cosine and sine evaluation. The number of words of computer memory required to do this is twice the number of digitization readings from the data photograph, typically

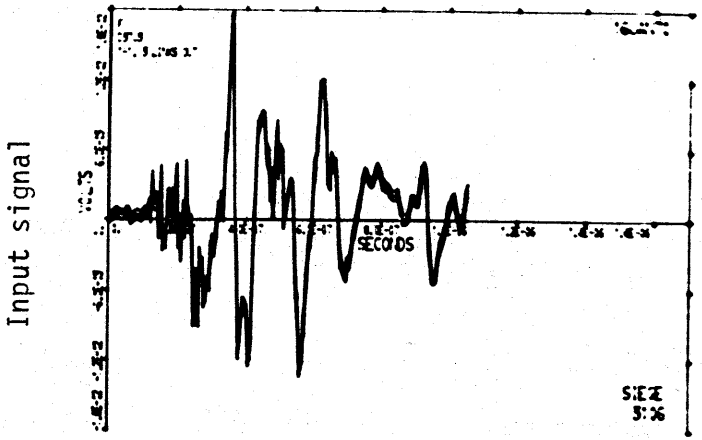

Figure 20.

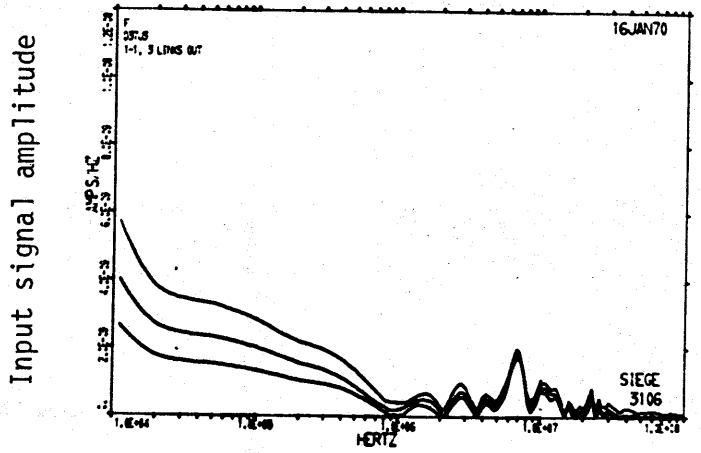

Figure 21.

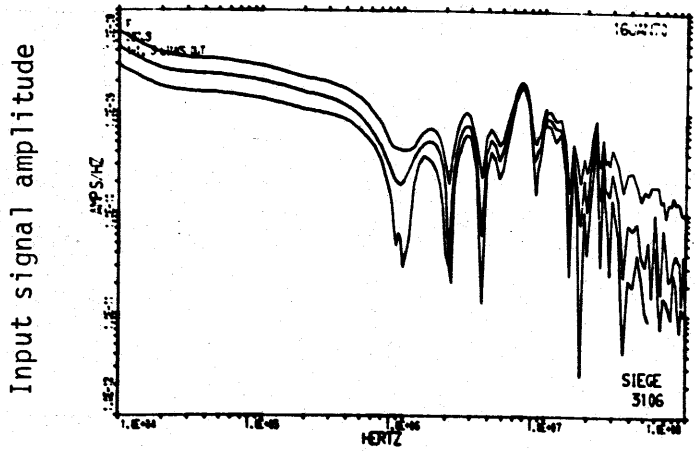

Figure 22.

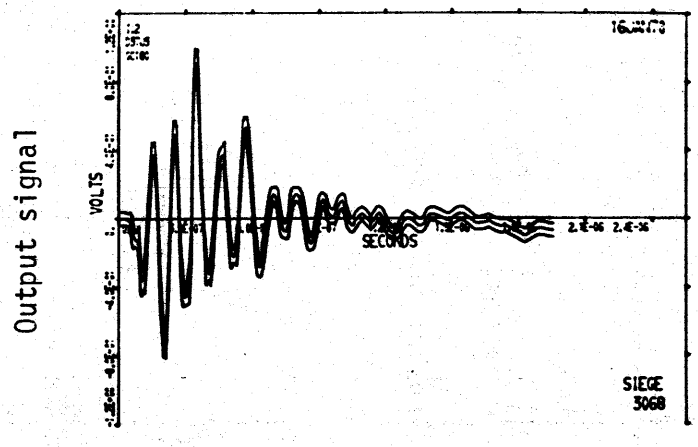

Figure 23.

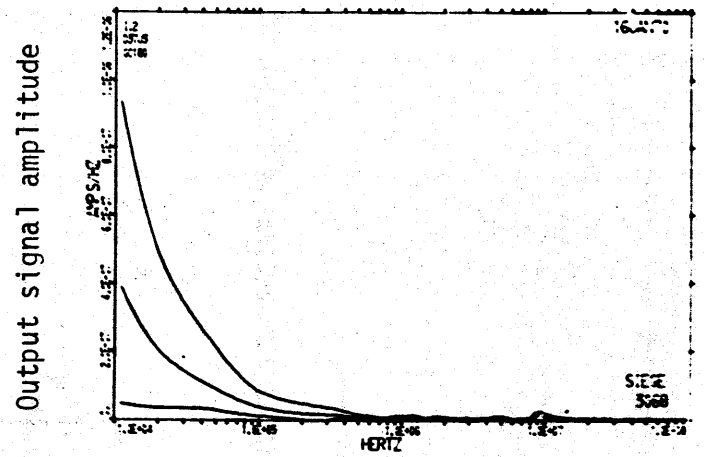

Figure 24.

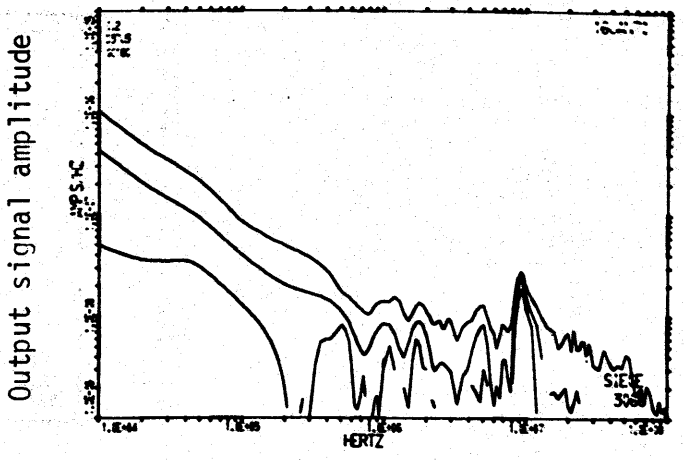

Figure 25.

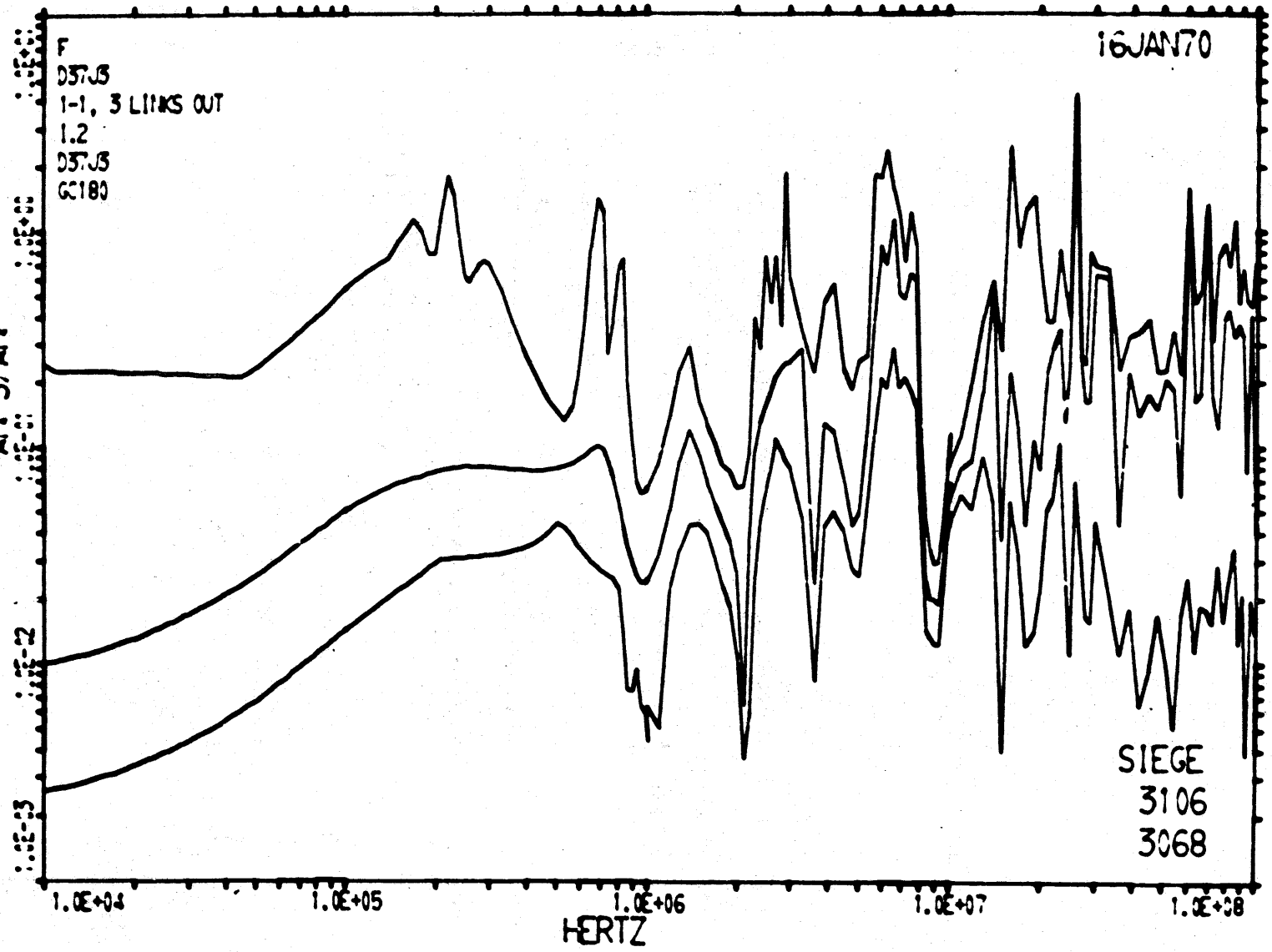

Figure 26. Transfer function amplitude

only a few hundred. Then proceed immediately, before changing frequency, to calculate all the pseudo-transforms and error bars at that frequency. In the subsequent pseudo-digitizations of that piece of data the values of X_i will not change (cf. paragraph 21 above). So the program can, for *all pseudo*-transforming, *look up* all quantities of the form $\cos \omega T_i$ or $\sin \omega T_i$, thus saving almost all the time otherwise required to evaluate trig series. (Of course, all the trig series will still have to be evaluated afresh when all the pseudo-transforming is complete at one frequency and a new frequency is embarked upon. This is true whether or not error bars are being calculated.[10])

Appendix A

Some sources of system test data distortion:

1. Spurious pseudo-signals; noise.
2. Sensor.
   - A. Transfer function.
   - B. Placement.
     - I. Orientation.
3. Integrator.
   - A. $1/(1+i\omega RC)$ transfer function.
     - I. $\sim 1/RC$ scaling.
     - II. Capacitor discharge ("integrator undershoot").
4. Balun.
5. Timing system.
6. Cables.
7. Amplifier.
   - A. Linearity.
   - B. Noise.
8. Attenuator.
   - A. Remote control.
9. Microwave relay system.
   - A. Transfer function (including temperature dependent dielectric constant).
10. Oscilloscope.
    - A. Common mode rejection.
    - B. Beam aim.
      - I. Placement (orientation) of deflection plates or yokes.
      - II. Power supply.
      - III. Linearity of vertical deflection.
      - IV. Linearity and triggering of horizontal sweep.
      - V. Calibration.
      - VI. Overshoot.
      - VII. Saturation recovery time.
    - C. Phosphor.
      - I. Sensitivity (beam intensity).
      - II. Bleeding (trace width; dynamic range).
    - D. Glass face.
      - I. Orientation (normal to centered beam).
      - II. Curvature.
      - III. Reticle.
    - E. Signal truncation.
11. Camera.
    - A. Lens.
      - I. Grinding (aberrations).
      - II. Placement (orientation).
      - III. Focus.

(11. Camera, continued.)

B. Film.
I. Placement (correct for lens focus).
II. Orientation (parallel to lens and oscilloscope face).
III. Emulsion.
a. Sensitivity.
i. Age.
ii. Temperature.
b. Bleeding.

12. Spurious film markings (scratches, etc.).
13. Digitization.
A. Translation.
B. Rotation.
C. Sensitivity.
D. Digital truncation.
E. Positive trace width.
F. Sampling frequency.
14. Numerical Fourier analysis.
A. Interpolation assumptions.
B. Periodicity assumptions (aliasing).
C. Digital truncation and round-off.
D. Instrument transfer function unfolding.
15. Operator procedures.
A. Equipment care and handling.
I. Calibration.
II. Shock (dropping).
B. Control settings.
C. Care of recordings
I. Data identification and logging.
D. Digitization.
E. Computer program accuracy.
F. Entry of supplementary data into computer.

Appendix B

Variables Analysis.

Take the view that information about a system must pass to the system analyst through a succession of devices, as in the following figure.

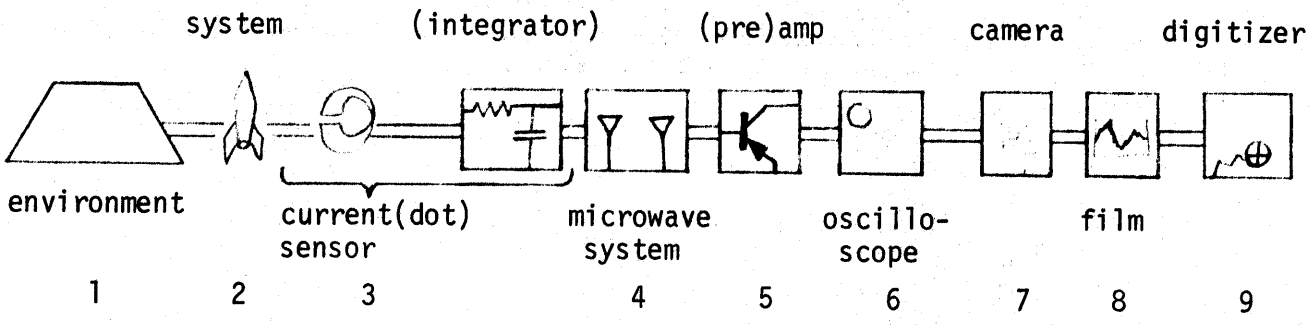

Define $T_i(\omega) \triangleq \frac{g(\omega)}{f(\omega)}$ (cf. Figure 1 and equation (4)) to be the transfer function, as a function of frequency ω, of the i^{th} approximately linear single-input-single-output component in such data transmission systems as that pictured above, where $1 \leq i \leq N$. Then the final value of $y(\omega)$ recorded is related to the true value $x(\omega)$ put into the system by the equation

$$y(\omega) = x(\omega) \prod_{i=1}^{N} T_i(\omega) .$$

We invert this relationship to recover $x(\omega)$:

$$x(\omega) = \frac{y(\omega)}{\prod_{i=1}^{N} T_i(\omega)} .$$

(Note that it is necessary that $T_i(\omega) \neq 0$ for all ω and for all i.) However, we can't really perform this calculation, since we don't know the $T_i(\omega)$ exactly. In practice we must use an approximation $A_i(\omega)$ for $T_i(\omega)$, so we recover instead:

$$w(\omega) \triangleq \frac{y(\omega)}{\prod_{i=1}^{N} A_i(\omega)}$$

Define $E(\omega) \triangleq \frac{w(\omega)}{x(\omega)}$; call this quotient the error in the estimate $w(\omega)$ of $x(\omega)$, since if we knew $E(\omega)$ we could divide it out and recover $x(\omega)$ accurately:

$$\frac{w(\omega)}{E(\omega)} = \frac{w(\omega)}{w(\omega)/x(\omega)} = x(\omega)$$

Define $B_i \triangleq 20 \log_{10}\left(\frac{T_i}{A_i}\right)$ dB. *Do whatever analysis and experimentation is necessary to discover the mean μ_i and the variance σ_i^2 of the distribution of each variable B_i.* Then note that

$$\begin{aligned}
E &= \log_{10}^{-1}(\log_{10} E) = \\
&= \log_{10}^{-1}\left(\log_{10}\frac{w}{x}\right) = \\
&= \log_{10}^{-1}\left(\log_{10}\frac{y/\Pi A_i}{y/\Pi T_i}\right) = \\
&= \log_{10}^{-1}\left(\log_{10}\frac{\Pi T_i}{\Pi A_i}\right) = \\
&= \log_{10}^{-1}\left[\log_{10}\left(\Pi\frac{T_i}{A_i}\right)\right] = \\
&= \log_{10}^{-1}\left[\Sigma\left(\log_{10}\frac{T_i}{A_i}\right)\right] = \\
&= \log_{10}^{-1}\left[\Sigma\left(20\log_{10}\frac{T_i}{A_i}\ \text{dB}\right)\right] = \\
&= \log_{10}^{-1}(\Sigma B_i)
\end{aligned}$$

The Central Limit Theorem[19] states that if the B_i are mutually independent

random variables with distributions (not necessarily the same) of known mean μ_i and variance σ_i^2, where the distributions satisfy the Lindeberg condition[19], then $\sum_{i=1}^{N} B_i$ will tend to the normal distribution with mean μ and variance σ^2 as N becomes large, where

$$\mu = \sum_{i=1}^{N} \mu_i \qquad \text{and} \qquad \sigma^2 = \sum_{i=1}^{N} \sigma_i^2$$

Therefore, if the B_i satisfy the Lindeberg condition, E will be log-normally distributed and we can calculate the values of the parameters of the distribution from the results of the analysis and experimentation recommended in the sentence italicized on the preceding page.

Finally, since

$$w(\omega) = x(\omega) * E(\omega)$$

and since $x(\omega)$ is a fixed (even if unknown) number, we conclude that the number $w(\omega)$ which we recover as our recorded data is really a log-normally distributed random variable and that the values of the parameters of the distribution are the same as those for E (again, provided N is sufficiently large and the B_i satisfy the Lindeberg condition).

Appendix C

Derivation of the vertical cross section c of the trace as a function of electron beam traversal speed s.

Model: $I = \frac{s_0}{s\tilde{\sigma}\sqrt{2\pi}} e^{-\frac{x^2}{2\tilde{\sigma}^2}}$ describes effective intensity of oscilloscope electron beam intensity, where x is distance $\perp$ to direction of beam travel and s is speed of beam travel. Then

$$I_0 = \frac{s_0}{s\tilde{\sigma}\sqrt{2\pi}} e^{\frac{-\left(\frac{w}{2}\right)^2}{2\tilde{\sigma}^2}} = \frac{s_0}{s\tilde{\sigma}\sqrt{2\pi}} e^{\frac{-w^2}{8\tilde{\sigma}^2}} \Longrightarrow$$

$$\Longrightarrow \frac{s_0}{s_1\tilde{\sigma}\sqrt{2\pi}} e^{\frac{-w_1^2}{8\tilde{\sigma}^2}} = \frac{s_0}{s_2\tilde{\sigma}\sqrt{2\pi}} e^{\frac{-w_2^2}{8\tilde{\sigma}^2}} \Longrightarrow$$

$$\Longrightarrow \frac{e^{-\frac{w_1^2}{8\tilde{\sigma}^2}}}{s_1} = \frac{e^{-\frac{w_2^2}{8\tilde{\sigma}^2}}}{s_2} \Longrightarrow$$

$$\Longrightarrow \frac{s_1}{s_2} = \frac{e^{-\frac{w_1^2}{8\tilde{\sigma}^2}}}{e^{-\frac{w_2^2}{8\tilde{\sigma}^2}}} = e^{\frac{w_2^2}{8\tilde{\sigma}^2} - \frac{w_1^2}{8\tilde{\sigma}^2}} = e^{\frac{w_2^2 - w_1^2}{8\tilde{\sigma}^2}} \Longrightarrow$$

$$\Longrightarrow \ln\frac{s_1}{s_2} = \frac{w_2^2 - w_1^2}{8\tilde{\sigma}^2} \Longrightarrow$$

$$\Longrightarrow \qquad \tilde{\sigma}^2 = \frac{w_2^2 - w_1^2}{8 \ln \frac{s_1}{s_2}}$$

Define $\tau \triangleq \dfrac{w_2^2 - w_1^2}{\ln \frac{s_1}{s_2}}$; then $\tau = 8\tilde{\sigma}^2$.

Then $$I_0 = \frac{s_0}{s\tilde{\sigma}\sqrt{2\pi}} e^{\frac{-w^2}{8\tilde{\sigma}^2}} \Longrightarrow$$

$$\Longrightarrow \quad I_0 = \frac{s_0}{s_1\tilde{\sigma}\sqrt{2\pi}} e^{\frac{-w_1^2}{\tau}} \quad \Lambda \quad \frac{I_0 s\tilde{\sigma}\sqrt{2\pi}}{s_0} = e^{\frac{-w^2}{\tau}} \Longrightarrow$$

$$\Longrightarrow \quad I_0 = \frac{s_0}{s_1\tilde{\sigma}\sqrt{2\pi}} e^{\frac{-w_1^2}{\tau}} \quad \Lambda \quad \ln\left(\frac{I_0 s\tilde{\sigma}\sqrt{2\pi}}{s_0}\right) = \frac{-w^2}{\tau} \Longrightarrow$$

$$\Longrightarrow \quad w^2 = -\tau \ln\left(\frac{I_0 s\tilde{\sigma}\sqrt{2\pi}}{s_0}\right)$$

$$= -\tau \ln\left(\frac{s\tilde{\sigma}\sqrt{2\pi}}{s_0} \frac{s_0}{s_1\tilde{\sigma}\sqrt{2\pi}} e^{\frac{-w_1^2}{\tau}}\right)$$

$$= -\tau \ln\left(\frac{s}{s_1} e^{-\frac{w_1^2}{\tau}}\right)$$

$$= w^2 = -\tau \left(\ell n \frac{s}{s_1} + \ell n\, e^{-\frac{w_1^2}{\tau}} \right)$$

$$= -\tau \left(\ell n \frac{s}{s_1} - \frac{w_1^2}{\tau} \right)$$

$$= \tau \left(\frac{w_1^2}{\tau} - \ell n \frac{s}{s_1} \right)$$

$$= w_1^2 - \tau\, \ell n \frac{s}{s_1}$$

By equation (10) in the text therefore,

$$c = (\sec \theta) \sqrt{w_1^2 - \tau\, \ell n \frac{s}{s_1}}$$

or, in the case of negative radicand, $c = 0$.

Appendix D

Procedures for calculating error bars.

I. Procedure for determining σ_i as a function of $\{(x_i, y_i)\}$.

1. Find two "straight" portions g_1 and g_2 (g for "graph") of the curve which have very different absolute values of slope from one another. For each g_k do the following:

   a. At 5 different abscissa values digitize the top and bottom edges of g_k to obtain the set $E = \{(x_{ki}, y_{kti}), (x_{ki}, y_{kbi}) \ni 1 \leq i \leq 5\}$ (E for "edges", t for "top", b for "bottom").
   b. Calculate the vertical cross-section v_k (v for "vertical") of g_k by calculating the average of the set of differences $\{y_{kti} - y_{kbi} \ni 1 \leq i \leq 5\}$.
   c. Least squares fit this set of 10 points in E with the quadratic $M_k(x) = a_k x^2 + b_k x + c_k$ (M for "middle" line). M_k should "parallel" g_k.
   d. Calculate the slope m_k of g_k by evaluating the first derivative of M_k near the mid-point of g_k, i.e., $m_k = 2a_k x_{k3} + b_k$.
   e. Calculate the angle θ_k of g_k as $\theta_k = \tan^{-1} m_k$.
   f. Calculate the width w_k (w for "width") of g_k as $w_k = v_k \cos \theta_k$.
   g. Calculate the sweep speed s_k (s for "speed") of the writing beam in g_k divided by the horizontal sweep speed as $s_k = \sec \theta_k$.

2. Calculate $\tau = \dfrac{w_2^2 - w_1^2}{\ell n \dfrac{s_1}{s_2}}$.

3. Calculate the slope m_i of the curve at any point (x_i, y_i) as the average of the first two differences about (x_i, y_i).

4. Calculate $r_i = \sec(\tan^{-1} m_i)$.

5. $\sigma_i = .215\, r_i \sqrt{w_1^2 - \tau\, \ell n \dfrac{r_i}{s_1}}$. (In the event that this radicand is non-positive, set $\sigma_i = \max\{\sigma_j\}$.)

II. Procedure for determining error bars for numerical calculations of the direct Fourier transform $F(\omega_j)$ of the function represented by $\{(x_i, y_i)\}$.

1. Perform the following for all values of the indexing variable k from 1 to 25:

   a. For all x_i use y_i as the mean and σ_i as calculated in the procedure on the preceding page to generate y_{ik} with the computer normal random number generator.

   b. Numerically Fourier transform the piecewise linear function represented by $\{(x_i, y_{ik})\}$ by means of the same algorithm used to calculate $F(\omega_j)$. Let $F_k(\omega_j)$ denote the result.

2. The top "error bar" of the Fourier transform graph is a graph of the points $(\omega_j, F_{max}(\omega_j))$, where $F_{max}(\omega_j) \triangleq \max\{F_k(\omega_j) \ni 1 \le k \le 25\}$. Similarly, the lower envelope is a graph of $F_{min}(\omega_j) \triangleq \min\{F_k(\omega_j)$ $1 \le k \le 25$. (In the event $F(\omega_j) \le F_{min}(\omega_j)$, for that ω_j the definition of $F_{min}(\omega_j)$ is changed to $F_{min}(\omega_j) \triangleq F(\omega_j) - .1[\max\{F_k(\omega_j) \ni 1 \le k \le 25\} - F(\omega_j)]$. Similarly, when so required define $F_{max}(\omega_j) = F(\omega_j) + .1[F(\omega_j) - \min\{F_k(\omega_j) \ni 1 \le k \le 25\}]$. Note: if these contingency provisions result in $F_{min}(\omega_j) < 0$, redefine $F_{min}(\omega_j) = 0$.)

III. Procedure for determining error bars for numerical calculations of transfer functions $T(\omega_j)$.

1. Follow steps 1a and 1b of the preceding procedure for both the output and input waveforms to generate $\{F_k(\omega_j), G_k(\omega_j) \ni 1 \le k \le 25\}$. From this set calculate $\{T_k(\omega_j) \ni 1 \le k \le 25\}$, where $T_k(\omega_j) = G_k(\omega_j)/F_k(\omega_j)$ (cf. equation (4)).

2. Follow step 2 of the preceding procedure using $\{T_k(\omega_j) \ni 1 \le k \le 25\}$ to generate $T_{max}(\omega_j)$ and $T_{min}(\omega_j)$. Graphs of these two functions are the error bars for transfer function graphs.

Footnotes

1. Cf. reference [R3], pp. 2, 3.

2. Cf. [R10], pp. 82, 83, especially equations (5-2) and (5-10).

3. This is the time convolution theorem. Cf. [R10], p. 26, equation (2-71).

4. Cf. [R10], p. 7, equation (2-3).

5. Cf. [R10], p. 84, equation (5-14).

6. Another procedure has been proposed which is somewhat different from the procedure and variations outlined in the text. This new procedure is called SEM (the Singularity Expansion Method); cf. EMP Interaction Note 88, by Dr Carl E. Baum, dated 11 December 1971. In using SEM one puts into the linear system an arbitrary test stimulus $\tilde{f}(t)$ and records both $\tilde{f}(t)$ and $\tilde{g}(t)$, as in steps I and II of the procedure in paragraph 8. Then one Laplace (instead of Fourier) transforms $\tilde{f}(t)$ and $\tilde{g}(t)$ at enough complex values of $s \equiv \alpha+i\omega$ to search out the principal singularities of those transforms. These two sets of singularities determine the entire Laplace transforms. Accordingly, these two sets of singularities determine a transfer function of a complex (as opposed to purely imaginary) variable for the linear system. With this SEM transfer function one may calculate the response of the linear system to stimuli with different angles of incidence than used for the test stimulus. If the angle of incidence is unchanged for a new f(t), then the transfer function of a purely imaginary variable is still contained in that of the complex variable, so the SEM approach still allows one to complete the procedures of paragraph 8 to discover g(t). -- For purposes of the present paper the point of interest is that SEM procedures also require transforming field test data, albeit Laplace instead of Fourier transforming, at enough complex values of s to discover the singularities of the transform. Consequently the problem raised in Part II of this paper exists for SEM procedures also. And the solution to that problem suggested by this paper should therefore aid in application of SEM procedures, too.

7. Cf. [R9], p. 7 and pp. 9 through 14, inclusive.

8. Cf. [R4], Part IV: "Conclusions and Recommendations".

9. That this is so is apparent from the necessity for the term "writing speed" among those who design, manufacture, and use oscilloscope-camera systems. The term means "the maximum spot speed which can be adequately photographed", or "the speed of the fastest trace the [recording] system will record" (cf. equation (10) in the text). Cf. [R2], pp. 3-16/4-1 ff. Or cf. [R8], pp. 173 to 175.

10. These remarks of course apply only when the person operating the digitizing machine chooses the points to be digitized. They don't apply when the digitizing machine is of a kind in which the operator tries to slide a cursor along the trace and the machine automatically digitizes at uniform horizontal intervals. For this latter kind of digitizing arrangement appropriate adjustments would have to be made to the simulation model which we are developing here. The same kind of observation about necessity for tailoring the model can be made for the case in which the digitizing machine is a microdensitometer which scans automatically. Of these three kinds of digitizing machines we are developing our example model around the first not because it is necessarily the best, most accurate, or most common, but because the experimental data of [R4] which we must use to validate our simulation idea was taken with the first kind of machine.

11. This assumes that the errors in one distribution in Figure 12 are wholly independent of the errors in all of the other distributions in that figure. Another way of stating this assumption is to say that the errors accumulated from the first thirteen sources in Appendix A yield a mutually independent discrete parameter stochastic process. However it is stated, the assumption is subject to experimental verification (i.e., statistical checks for independence). We (the authors) are unaware of any such verification to date. Pending report of such verification, however, we believe the assumption to be sufficiently accurate to allow us to proceed with the error estimation procedure being developed in this paper.

12. This is Figure 9 in [R4]. -- "DFDT", the vertical axis label in Figure 19, is explained in [R4] to mean the *absolute value* of the first time derivative of the data. This derivative is in "engineering units", such as volts/second, not in the units of the trace slope m (viz., cm/cm). The trace slope m is not given in [R4] for the data which generated Figure 19. However, to the degree that the oscilloscope is a linear instrument, the slope of the trace is simply the derivative of the data multiplied by scaling constants with appropriate units. We have been equally unsuccessful at discovering the values of these scaling factors from [R4].

13. One would prefer to make a quantitative argument. For the moderate values of $|m|$ which we believe to be represented in Figure 19, a quantitative argument might begin in this way. The hypothesis contained in equation (16) states that $\sigma \doteq k*c$. Invoking the estimate in equation (17), the hypothesis becomes $\sigma \doteq .215*c$. According to Figure 18, for small values of $|m|$ (say, $|m| < 12$), $c \doteq [(.71/12)|m|+.1]$ cm $\doteq (.059|m|+.1)$ cm. Therefore combining the information from Figure 18 with the hypothesis yields $\sigma \doteq .215*c \doteq .215*(.059|m|+.1)$ cm $\doteq (.0127|m|+.0215)$ cm. It should be possible to compare the estimate $\sigma \doteq (.0127|m|+.0215)$ cm, which is based upon the hypothesis contained in equation (16), with the experimentally determined relationship between σ and $|m|$ shown in Figure 19. Unfortunately we cannot at present complete this quantitative argument, for two reasons. First, we have not been able to determine values for the slope and bias of the (generally linear) experimental function in Figure 19 because of the missing scaling factors (cf. footnote 12,

above). Second, the photograph parameter values used to construct Figure 18 are merely *typical*, round numbers, not at all necessarily identically the same as those of the data photographs which produced Figure 19 (Figure 9 in [R4]). The values of the parameters of equation (14) for the latter real photographs were not available to the authors during preparation of the present paper, since they were not included in [R4] and the authors of the present paper do not at present have the photographs themselves.

14. Cf. [R6], pp. 197 to 199, especially equation (22-10). Or cf. [R7], pp. 220, 221. Or cf. [R1], pp. 18, 19, especially equation (13).

15. Cf. [R7], p. 293, Theorem AII.2.

16. Cf. [R7], p. 302, Corollary.

17. Cf. [R5], p. 47.

18. Cf. [R7], p. 307, Theorem AVI.10.

19. Cf. [R5], p. 256.

20. This report is actually named somewhat erroneously, since the digitizer used would more accurately be described as semi-automatic than manual. The human operator positioned the crosshairs manually, but at the touch of a button the coordinates of the crosshairs were read, digitized, and recorded automatically. This difference is significant for the present paper since it means the detailed example of the error simulation technique which we develop here does *not* include the error a human commonly makes in reading precise coordinates due to early, unrelieved boredom. The absence of this error source is assumed by paragraph 19 in the text.

References

[R1] Chris Ashley, *Confidence and Reliability in an Infinite Population.* EMP System Design and Assessment Note 3; 7 October 1971.

[R2] Robert A. Bell, *Principles of Cathode-ray Tubes, Phosphors, and High-speed Oscillography.* Hewlett-Packard Application Note 115; copyright 1970.

[R3] David K. Cheng, *Analysis of Linear Systems.* Addison-Wesley Publishing Company, Inc.; copyright 1959.

[R4] Linda L. Doran and L. Carlisle Nielsen, *A Study of the Errors in the Manual Digitization of Oscilloscope Trace Photographs*[20]. Contract report prepared for the Air Force Weapons Laboratory by EG&G, Inc.; July 1970.

[R5] William Feller, *An Introduction to Probability Theory and Its Applications,* Volume II. John Wiley & Sons, Inc.; copyright 1966.

[R6] Harold Freeman, *Introduction to Statistical Inference.* Addison-Wesley Publishing Company, Inc.; copyright 1963.

[R7] Irwin Guttman and S. S. Wilks, *Introductory Engineering Statistics.* John Wiley & Sons, Inc.; copyright 1965.

[R8] Will Marsh, *Oscilloscope Camera Concepts.* Tektronix, Inc.; copyright 1973.

[R9] Amber McEwen, *Transfer Function Error Analysis.* Contract report prepared for the Air Force Weapons Laboratory by EG&G, Inc.; 11 May 1970.

[R10] Athanasios Papoulis, *The Fourier Integral and Its Applications.* McGraw-Hill Book Company, Inc.; copyright 1962.

Definitions of symbols

Symbol	Meaning
$\triangleq$	is defined to mean
$\Longrightarrow$	implies
$\Longleftrightarrow$	implies and is implied by
$\wedge$	logical "AND"
$\equiv$	is identically the same as
$\doteq$	is approximately equal to
(x,y)	a pair, or "two-tuple", giving the coordinates of a point in two dimensional space; also stands for the point itself
$\{a,b,\ldots,z\}$	the *set* containing the elements a,b,...,z
$\cup$	union (of two sets)
$\ni$	such that
$\perp$	is perpendicular to
$\lvert a \rvert$	the absolute value of a
*	"times" (i.e., ordinary multiplication; this operation is also indicated in some places by juxtaposition)
$\prod_{i=1}^{N} x_i$	the product $x_1 * x_2 * \cdots * x_N$ (products are also indicated by the same symbol typed: Π)
ℓn	the natural, or Naperian, logarithm (base e)